

## Ru (II) Complexes with Diazine Ligands: Electronic Modulation of Coordinating Group is Key to the Design of “Dual Action” Photoactivated Agents

Dmytro Havrylyuk, Megha Deshpande, Sean Parkin, and Edith C. Glazer\*

Department of Chemistry, University of Kentucky, 505 Rose Street, Lexington, Kentucky 40506, United States

Department of Chemistry, University of Kentucky, Lexington, KY 40506, United States.

Supplementary Information

### 1. Materials and instrumentation.

**Table S1:** HPLC gradient used for determination of purity and photoejection products.

### 2. Synthesis and characterization of *cis*-[Ru(bpy)<sub>2</sub>L<sub>2</sub>]<sup>2+</sup> (1–4).

**Chart S1.** Labeling of the protons for compounds 1–4.

### 3. Synthesis and characterization of *trans*-[Ru(qpy)(pyz)<sub>2</sub>]<sup>2+</sup> (7), and *cis*-[Ru(tpy)(bpy)(L)]<sup>2+</sup> (8, 9).

**Table S2:** <sup>1</sup>H NMR chemical shifts (ppm) of bpy, pyridine (1) and diazine (2–4) resonances.

### 4. Photoejection studies.

**Table S3:** Half-lives of second ligand ejection for 2–4 determined under different buffer conditions.

### 5. DNA damage assay.

### 6. Additional Figures and Tables.

**Figure S1.** Ellipsoid plot of ruthenium complexes 2 and 3.

**Table S4.** Selected bond lengths (Å) and bond angles (°) of 2 and 3 in comparison with 1.

**Figure S2.** Photoejection of 50 μM 1 in water for 0-240 min irradiation.

**Figure S3.** Photoejection of 50 μM 2 in water for 0-240 min irradiation.

**Figure S4.** Photoejection of 50 μM 3 in water for 0-240 min irradiation.

**Figure S5.** Photoejection of 50 μM 4 in water for 0-240 min irradiation.

**Figure S6.** Determination of photoejection products by HPLC for 3.

**Figure S7.** Determination of photoejection products by HPLC for 4.

**Figure S8.** Agarose gel electrophoresis for 1–4.

**Figure S9.** Photoejection of 6 (A, B) and 7 (C, D) in water for 0–540 min irradiation monitored by UV/Vis absorbance and HPLC.

**Figure S10.** <sup>1</sup>H NMR of 1 in CD<sub>3</sub>CN.

**Figure S11.** <sup>1</sup>H NMR of 2 in CD<sub>3</sub>CN.

**Figure S12.** <sup>13</sup>C NMR of 2 in CD<sub>3</sub>CN.

**Figure S13.** <sup>1</sup>H NMR of 3 in CD<sub>3</sub>CN.

**Figure S14.** <sup>13</sup>C NMR of 3 in CD<sub>3</sub>CN.

**Figure S15.** <sup>1</sup>H NMR of 4 in CD<sub>3</sub>CN.

**Figure S16.** <sup>13</sup>C NMR of 4 in CD<sub>3</sub>CN.

**Figure S17.** <sup>1</sup>H NMR of 7 in DMSO.

**Figure S18.** <sup>13</sup>C NMR of 7 in DMSO.

**Figure S19.** <sup>1</sup>H NMR of 8 in CD<sub>3</sub>CN.

**Figure S20.** <sup>1</sup>H NMR of 9 in CD<sub>3</sub>CN.

**Figure S21.** Stability of complexes 2–4, 7, and 9 in different media in the dark over 0-72 h.

**7. Detailed methods for determination of quantum yields.** Illustrative tables and figures are included (Scheme S1, Tables S5-S13, Figures S22-S28).

## 1. Materials and instrumentation.

All materials were purchased from commercial sources and used without any further purification. All  $^1\text{H-NMR}$  and  $^{13}\text{C-NMR}$  were obtained on a Varian Mercury spectrometer (400, 100MHz) and chemical shifts are reported relative to the residual solvent peak of  $\text{CD}_3\text{CN}$  ( $\delta$  1.94 (1H) or 1.39 ( $^{13}\text{C}$ )). Electrospray ionization (ESI) mass spectra were obtained on a Varian 1200L mass spectrometer at the Environmental Research Training Laboratory (ERTL) at the University of Kentucky. UV/Vis absorption spectra were obtained on a BMG Labtech FLUOstar Omega microplate reader. Light activation experiments were performed using a 470 nm LED array from Elixia. The Prism software package was used to analyze data. Compound **5**<sup>1</sup> and **6**<sup>2</sup> have been reported previously.

**HPLC analysis for purity and photoejection products:** The purity of each Ru(II) complex and photoejection products of **1–4** and **5** were analyzed using an Agilent 1100 Series HPLC equipped with a model G1311A quaternary pump, G1315B UV diode array detector and Chemstation software version B.01.03. Chromatographic conditions were optimized on a Column Technologies Inc. C18 120 Å column fitted with a Phenomenex C18 guard column. Mobile phases of 0.1% formic acid in  $\text{dH}_2\text{O}$  and 0.1% formic acid in HPLC grade  $\text{CH}_3\text{CN}$  were used. Samples of each Ru(II) complex were prepared at a final concentration of 500  $\mu\text{M}$  in  $\text{dH}_2\text{O}$  and protected from light (dark controls/purity analysis) or irradiated to determine the photoejection products.

**Table S1:** HPLC gradient used for compound purity and adduct formation.

Time (min)	% $\text{dH}_2\text{O}$ (0.1% formic acid)	% $\text{CH}_3\text{CN}$ (0.1% formic acid)
0	98	2
2	95	5
5	95	5
10	90	10
20	90	10
25	70	30
30	40	60
35	5	95
40	98	2
45	98	2

## 2. Synthesis and characterization of *cis*-[Ru(bpy)<sub>2</sub>L<sub>2</sub>]<sup>2+</sup> (**1–4**).

*cis*-Ru(bpy)<sub>2</sub>Cl<sub>2</sub> (0.15 g, 0.288 mmol) and 10-fold excess (2.88 mmol) of pyridine or diazine (pyridazine – pyd, pyrimidine – pym, pyrazine – pyz) were added to 10 mL of degassed ethanol:water (1:1) in a 25 mL round bottom flask. The mixture was stirred under reflux for 12 hours. The reaction was allowed to cool to room temperature, excess starting material was extracted into dichloromethane, and a saturated aqueous solution of KPF<sub>6</sub> (1–2 mL) was added to the aqueous fraction, producing a red precipitate. The precipitate was then extracted into dichloromethane, and the solvent removed under reduced pressure. Purification of the solid was performed using flash chromatography ( $\text{SiO}_2$ , 0.3% saturated  $\text{KNO}_3$ , 5% water in  $\text{CH}_3\text{CN}$ , ramped to 15%  $\text{H}_2\text{O}$ ) to give the pure complex. After column purification, the  $\text{NO}_3^-$ -salt was dissolved in minimal water and converted to the  $\text{PF}_6^-$ -salt upon the addition of a saturated solution of KPF<sub>6</sub>. The precipitate was isolated by extraction into dichloromethane and the solvent was removed under reduced pressure.

*cis*-[Ru(bpy)<sub>2</sub>(py)<sub>2</sub>]<sup>2+</sup> (**1**) Yield: 230 mg (92%). <sup>1</sup>H NMR (CD<sub>3</sub>CN): δ 8.90 (d, *J* = 5.2 Hz, 2H, 6'-bpy), 8.35 (d, *J* = 8.0 Hz, 2H, 3'-bpy), 8.26-8.29 (m, 6H, 3-bpy, α-py), 8.13 (td, *J* = 8.0, 1.5 Hz, 2H, 4'-bpy), 7.89-7.94 (m, 4H, 4,6-bpy), 7.85 (tt, *J* = 7.7, 1.5 Hz, 2H, γ-py), 7.76 (ddd, *J* = 8.0, 5.7, 1.4 Hz, 2H, 5'-bpy), 7.35 (ddd, *J* = 8.0, 5.8, 1.3 Hz, 2H, 5-bpy), 7.27-7.31 (m, 4H, β-py); purity by HPLC = 95 %; UV/Vis (CH<sub>3</sub>CN): λ<sub>max</sub> (ε × 10<sup>-3</sup>) 455 nm (8.9).

*cis*-[Ru(bpy)<sub>2</sub>(pyd)<sub>2</sub>]<sup>2+</sup> (**2**) Yield: 230 mg (92%). <sup>1</sup>H NMR (CD<sub>3</sub>CN): δ 8.97 (d, *J* = 5.6 Hz, 2H, 6'-bpy), 8.93-8.96 (m, 2H, α-pyd), 8.80 (dt, *J* = 5.8, 1.2 Hz, 2H, δ-pyd), 8.36 (d, *J* = 7.9 Hz, 2H, 3'-bpy), 8.23 (d, *J* = 8.1 Hz, 2H, 3-bpy), 8.15 (td, *J* = 8.0, 1.5 Hz, 2H, 4'-bpy), 7.89 (td, *J* = 8.0, 1.5 Hz, 2H, 4-bpy), 7.84 (d, *J* = 5.8 Hz, 2H, 6-bpy), 7.76 (ddd, *J* = 8.0, 5.7, 1.4 Hz, 2H, 5'-bpy), 7.63 (ddd, *J* = 8.8, 5.0, 1.4 Hz, 2H, β-bpy), 7.48 (ddd, *J* = 8.0, 5.8, 2.0 Hz, 2H, γ-pyd), 7.31 (ddd, *J* = 8.0, 5.6, 1.3 Hz, 2H, 5-bpy); <sup>13</sup>C NMR (CD<sub>3</sub>CN): δ 158.62, 158.47, 158.13, 154.53, 153.86, 153.70, 139.08, 138.74, 131.31, 128.45, 127.81, 124.65, 124.09; purity by HPLC = 98 %; ESI MS calcd for C<sub>28</sub>H<sub>24</sub>N<sub>8</sub>Ru [M]<sup>+</sup> PF<sub>6</sub><sup>-</sup> 719.08, [M]<sup>2+</sup> 287.06; found 719.2 [M]<sup>+</sup> PF<sub>6</sub><sup>-</sup>, 287.0 [M]<sup>2+</sup>; UV/Vis (CH<sub>3</sub>CN): λ<sub>max</sub> (ε × 10<sup>-3</sup>) 420 nm (12.5).

*cis*-[Ru(bpy)<sub>2</sub>(pym)<sub>2</sub>]<sup>2+</sup> (**3**) Yield: 240 mg (96%). <sup>1</sup>H NMR (CD<sub>3</sub>CN): δ 8.95 (t, *J* = 1.2 Hz, 2H, δ-pym), 8.89 (d, *J* = 5.2 Hz, 2H, 6'-bpy), 8.79 (dd, *J* = 5.4, 2.1 Hz, 2H, α-pym), 8.53 (ddd, *J* = 6.4, 1.9, 1.3 Hz, 2H, γ-pym), 8.39 (d, *J* = 8.2 Hz, 2H, 3'-bpy), 8.29 (d, *J* = 8.1 Hz, 2H, 3-bpy), 8.18 (td, *J* = 8.0, 1.5 Hz, 2H, 4'-bpy), 7.95 (td, *J* = 8.0, 1.5 Hz, 2H, 4-bpy), 7.86 (d, *J* = 5.5 Hz, 2H, 6-bpy), 7.80 (ddd, *J* = 8.0, 5.7, 1.4 Hz, 2H, 5'-bpy), 7.36-7.40 (m, 4H, 5-bpy, β-pym); <sup>13</sup>C NMR (CD<sub>3</sub>CN): δ 162.57, 161.73, 159.22, 158.70, 158.66, 153.71, 153.25, 139.45, 139.13, 129.17, 128.83, 125.47, 125.01, 124.10; purity by HPLC = 96 %; ESI MS calcd for C<sub>28</sub>H<sub>24</sub>N<sub>8</sub>Ru [M]<sup>+</sup> PF<sub>6</sub><sup>-</sup> 719.08, [M]<sup>2+</sup> 287.06; found 719.3 [M]<sup>+</sup> PF<sub>6</sub><sup>-</sup>, 286.9 [M]<sup>2+</sup>; UV/Vis (CH<sub>3</sub>CN): λ<sub>max</sub> (ε × 10<sup>-3</sup>) 435 nm (9.6).

*cis*-[Ru(bpy)<sub>2</sub>(pyz)<sub>2</sub>]<sup>2+</sup> (**4**) Yield: 220 mg (88%). <sup>1</sup>H NMR (CD<sub>3</sub>CN): δ 8.83 (d, *J* = 5.2 Hz, 2H, 6'-bpy), 8.45-8.46 (m, 4H, α-pyz), 8.38 (d, *J* = 8.0 Hz, 2H, 3'-bpy), 8.28-8.31 (m, 6H, 3-bpy, β-pyz), 8.18 (td, *J* = 8.0, 1.5 Hz, 2H, 4'-bpy), 7.97 (td, *J* = 8.0, 1.5 Hz, 2H, 4-bpy), 7.80-7.84 (m, 4H, 5',6-bpy), 7.40 (ddd, *J* = 8.0, 5.7, 1.4 Hz, 2H, 5-bpy); <sup>13</sup>C NMR (CD<sub>3</sub>CN): δ 158.43, 158.31, 153.46, 153.09, 149.77, 147.94, 139.68, 139.45, 129.31, 128.99, 125.46, 125.00; purity by HPLC = 95 %; ESI MS calcd for C<sub>28</sub>H<sub>24</sub>N<sub>8</sub>Ru [M]<sup>+</sup> PF<sub>6</sub><sup>-</sup> 719.08, [M]<sup>2+</sup> 287.06; found 719.3 [M]<sup>+</sup> PF<sub>6</sub><sup>-</sup>, 287.0 [M]<sup>2+</sup>; UV/Vis (CH<sub>3</sub>CN): λ<sub>max</sub> (ε × 10<sup>-3</sup>) 415 nm (8.7).

### 3. Synthesis and characterization of *trans*-[Ru(qpy)(pyz)<sub>2</sub>]<sup>2+</sup> (**7**) and *cis*-[Ru(tpy)(bpy)(L)]<sup>2+</sup> (**8**, **9**).

*trans*-[Ru(qpy)(pyz)<sub>2</sub>](PF<sub>6</sub>)<sub>2</sub> (**7**): To a suspension of Ru(qpy)Cl<sub>2</sub>•3.5 H<sub>2</sub>O (35 mg, 0.073 mmol) in EtOH:H<sub>2</sub>O (4:1) an excess of pyrazine (120 mg, 1.5 mmol) was added under N<sub>2</sub>. The resulting mixture was refluxed at 90 °C overnight. After cooling the orange solution to 22 °C, 1–2 mL of a saturated aqueous KPF<sub>6</sub> solution was added to obtain an orange precipitate that was extracted with CH<sub>2</sub>Cl<sub>2</sub>/CH<sub>3</sub>CN (3 x 10 mL). The organic phase was further purified by flash chromatography (SiO<sub>2</sub> eluting at 80:20:0.4 acetonitrile/water/saturated KNO<sub>3</sub>). The solvent was removed under vacuum, and the complex was converted to PF<sub>6</sub><sup>-</sup> salt. Yield: 35 mg (66%). <sup>1</sup>H NMR (DMSO): δ 9.93 (d, *J* = 4.8 Hz, 2H), 8.91 (d *J* = 8.0 Hz, 2H), 8.63 (d, *J* = 8.1 Hz, 2H), 8.50 (d, *J* = 8.1 Hz, 2H), 8.24-8.32 (m, 8H), 8.16-8.17 (m, 4H), 8.01 (t, *J* = 6.4 Hz, 2H); <sup>13</sup>C NMR (DMSO): δ 158.64, 158.47, 157.62, 154.83, 146.53, 146.29, 140.38, 137.02, 129.49, 126.03, 124.43, 124.33; purity by HPLC = 99 %; ESI MS calcd for C<sub>28</sub>H<sub>24</sub>N<sub>8</sub>Ru [M]<sup>2+</sup> 286.05; found 286.0 [M]<sup>2+</sup>; UV/Vis (CH<sub>3</sub>CN): λ<sub>max</sub> (ε × 10<sup>-3</sup>) = 285 nm (32.2), 335 nm (14.0), 350 nm (16.1), 380 nm (11.0), 495 nm (4.9).

*cis*-[Ru(tpy)(bpy)(py)]<sup>2+</sup> (**8**) To a suspension of Ru(tpy)(bpy)Cl (150 mg, 0.267 mmol) in EtOH:H<sub>2</sub>O (4:1) an excess of pyridine (1.4 ml, 17 mmol) was added under N<sub>2</sub>. The resulting mixture was refluxed at 90 °C overnight. After cooling the red solution to 22 °C, the excess of pyridine was extracted with CH<sub>2</sub>Cl<sub>2</sub>, and further 1–2 mL of a saturated aqueous KPF<sub>6</sub> solution was added to obtain a red precipitate that was extracted with CH<sub>2</sub>Cl<sub>2</sub> (3 x 10 mL). The organic phase was concentrated under vacuum and precipitated with ether. The solvent was removed by filtration. Yield: 160 mg (72%). <sup>1</sup>H NMR (CD<sub>3</sub>CN): δ 8.67 (d, *J* = 7.0 Hz, 2H), 8.52 (d, *J* = 8.1 Hz, 2H), 8.39-8.44 (m, 3H), 8.31 (t, *J* = 8.0 Hz, 1H), 8.20 (t, *J* = 8.2 Hz, 1H), 8.02 (t, *J* = 7.8 Hz, 2H), 7.76-7.85 (m, 5H), 7.69 (d, *J* = 5.7 Hz, 2H), 7.41 (t, *J* = 6.4 Hz, 2H), 7.27 (d, *J* = 5.6 Hz, 1H), 7.21 (t, *J* = 6.6 Hz, 2H), 7.08 (t, *J* = 6.6 Hz, 1H); <sup>13</sup>C NMR (CD<sub>3</sub>CN): δ: 158.91, 158.31, 158.13, 157.04, 153.76, 152.86, 152.44, 152.01, 139.51, 139.15, 138.58, 138.27, 137.01, 129.59, 128.60, 127.69, 127.34, 125.95, 125.51, 124.94, 124.72. purity by HPLC = 98 %; ESI MS calcd for C<sub>30</sub>H<sub>24</sub>N<sub>6</sub>Ru [M]<sup>+</sup> PF<sub>6</sub><sup>-</sup> 715.1, [M]<sup>2+</sup> 285.1; found 715.1 [M]<sup>+</sup> PF<sub>6</sub><sup>-</sup>, 285.0 [M]<sup>2+</sup>; UV/Vis (CH<sub>3</sub>CN): λ<sub>max</sub> (ε × 10<sup>-3</sup>) 465 nm (8.8).

*cis*-[Ru(tpy)(bpy)(pyz)]<sup>2+</sup> (**9**) Ru(tpy)(bpy)Cl (60 mg, 0.1 mmol), 5-fold excess of pyrazine (40 mg, 0.5 mmol) and AgNO<sub>3</sub> (34 mg, 0.2 mmol) were added to 6 mL of degassed ethanol:water (2:1) in a pressure tube. The mixture was stirred at 80 °C for 12 hours. The reaction was allowed to cool to room temperature and excess of pyrazine was extracted with CH<sub>2</sub>Cl<sub>2</sub>. Next, 1–2 mL of a saturated aqueous solution of KPF<sub>6</sub> was added to the aqueous fraction, and product was extracted with CH<sub>2</sub>Cl<sub>2</sub>. The organic phase was concentrated under vacuum and precipitated with ether. The red product was isolated by filtration and washed with ether. Yield: 32 mg (37%). <sup>1</sup>H NMR (CD<sub>3</sub>CN): δ 8.71 (d, *J* = 5.7 Hz, 2H), 8.67 (d, *J* = 8.2 Hz, 2H), 8.53 (d, *J* = 8.2 Hz, 2H), 8.40-8.44 (m, 3H), 8.30-8.35 (m, 3H), 8.24 (t, *J* = 8.2 Hz, 1H), 8.04 (t, *J* = 7.8 Hz, 2H), 7.84 (t, *J* = 7.2 Hz, 2H), 7.74-7.77 (m, 4H), 7.42 (t, *J* = 7.5 Hz, 2H), 7.26 (d, *J* = 5.6 Hz, 1H), 7.10 (t, *J* = 6.6 Hz, 1H); <sup>13</sup>C NMR (DMSO): δ 157.13, 156.53, 156.10, 155.28, 152.23, 150.81, 150.16, 146.37, 146.02, 137.92, 136.98, 136.74, 135.77, 127.77, 126.74, 125.88, 124.14, 123.62, 123.17, 122.80; purity by HPLC = 99 %; ESI MS calcd for C<sub>29</sub>H<sub>23</sub>N<sub>7</sub>Ru [M]<sup>+</sup> PF<sub>6</sub><sup>-</sup> 716.07, [M]<sup>2+</sup> 285.56; found 716.1 [M]<sup>+</sup> PF<sub>6</sub><sup>-</sup>, 285.4 [M]<sup>2+</sup>; UV/Vis (CH<sub>3</sub>CN): λ<sub>max</sub> (ε × 10<sup>-3</sup>) 430 nm (10.0).

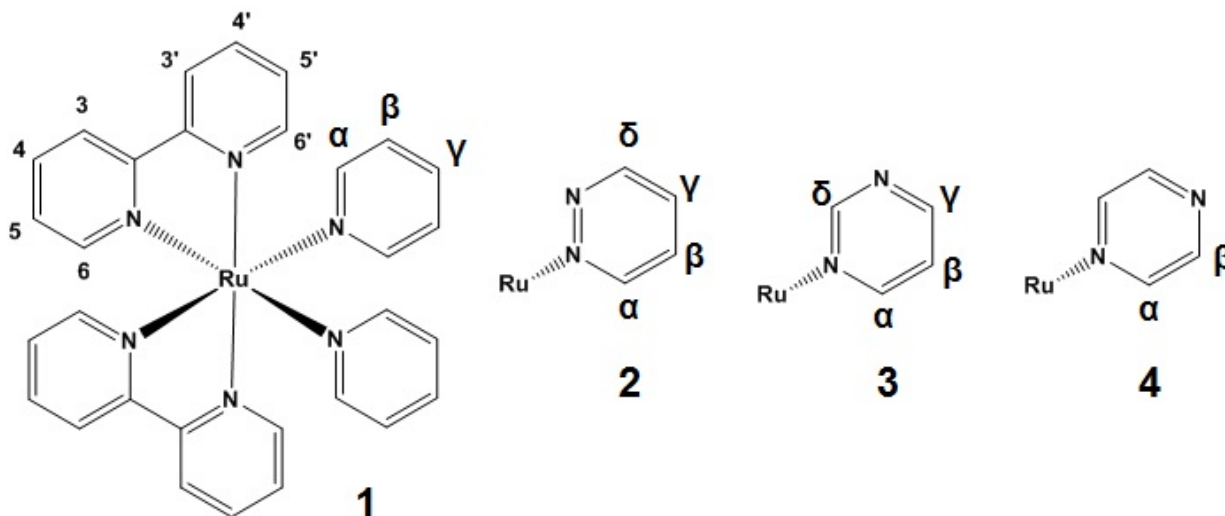


**Chart S1.** Labeling of the protons for compounds 1–4.

**Table S2:** <sup>1</sup>H NMR chemical shifts (ppm) of bpy, pyridine (**1**) and diazine (**2–4**) resonances.

Comp	Signal	1	2	3	4
6'	d	8.90	8.97	8.89	8.83
3'	d	8.35	8.36	8.39	8.38
3	d	8.26-8.29	8.23	8.29	8.28-8.31
4'	td	8.13	8.15	8.18	8.18
4	td	7.89-7.94	7.89	7.95	7.97
6	d		7.84	7.86	7.80-7.84
5'	ddd	7.76	7.76	7.80	
5	ddd	7.35	7.31	7.36-7.40	7.40
α		8.26-8.29	8.93-8.96	8.79	8.45-8.46
β		7.27-7.31	7.63	7.36-7.40	8.28-8.31
γ		7.85	7.48	8.53	
δ		-	8.80	8.95	-

### Crystallography

Single crystals of compound **2** were grown from acetonitrile by vapor diffusion of diethyl ether, the mounted in inert oil and transferred to the cold gas stream of the diffractometer. X-ray diffraction data were collected at 90.0(2) K on a Bruker-Nonius X8 Proteum diffractometer with graded-multilayer focused CuK $\alpha$  X-rays. Raw data were integrated, scaled, merged and corrected for Lorentz-polarization effects using the APEX2 package (2).<sup>3</sup> Corrections for absorption were applied using SADABS<sup>4</sup> and XABS2.<sup>5</sup> The structures were solved by SHELXT,<sup>6</sup> and refined against F<sup>2</sup> by weighted full-matrix least-squares using SHELXL.<sup>7</sup> Hydrogen atoms were placed at calculated positions and refined using a riding model. Non-hydrogen atoms were refined with anisotropic displacement parameters. Structure was checked using check CIF tools in Platon<sup>8</sup> and by an R-tensor.<sup>9</sup> Crystal data and relevant details of the structure determinations are summarized below and selected geometrical parameters are given in Table S12.

**Crystal data (2):** C<sub>28</sub>H<sub>24</sub>F<sub>12</sub>N<sub>8</sub>P<sub>2</sub>Ru, Mr = 863.56, Monoclinic, C2/c, a = 13.5829(4) Å,  $\alpha$  = 90°, b = 20.0799(5) Å,  $\beta$  = 90.845(1)°, c = 11.5630(3) Å,  $\gamma$  = 90°, V = 3153.39(15) Å<sup>3</sup>, Z = 4,  $\rho$  = 1.819 Mg m<sup>-3</sup>,  $\mu$  = 5.981 mm<sup>-1</sup>, F(000) = 1720, crystal size = 0.110×0.090×0.070 mm,  $\theta$ (max) = 68.294°, 21425 reflections collected, 2884 unique reflections (R<sub>int</sub> = 0.0362), GOF = 1.110, R<sub>1</sub> = 0.0219 and wR<sub>2</sub> = 0.0605 [I > 2 $\sigma$ (I)], R<sub>1</sub> = 0.0221 and wR<sub>2</sub> = 0.0608 (all indices), largest difference peak/hole = 0.404/ -1.427 eÅ<sup>-3</sup>.

**Crystal data (3):** C<sub>28</sub>H<sub>24</sub>F<sub>12</sub>N<sub>8</sub>P<sub>2</sub>Ru, Mr = 863.56, Monoclinic, C2/c, a = 21.4835(4) Å,  $\alpha$  = 90°, b = 10.2495(2) Å,  $\beta$  = 125.539(1)°, c = 17.1972(4) Å,  $\gamma$  = 90°, V = 3081.34(11) Å<sup>3</sup>, Z = 4,  $\rho$  = 1.861 Mg m<sup>-3</sup>,  $\mu$  = 6.121 mm<sup>-1</sup>, F(000) = 1720, crystal size = 0.070×0.050×0.030 mm,  $\theta$ (max) = 68.298°, 20116 reflections collected, 2816 unique reflections (R<sub>int</sub> = 0.0532), GOF = 1.076, R<sub>1</sub> = 0.0346 and wR<sub>2</sub> = 0.0885 [I > 2 $\sigma$ (I)], R<sub>1</sub> = 0.0402 and wR<sub>2</sub> = 0.0911 (all indices), largest difference peak/hole = 0.555 / -0.53 eÅ<sup>-3</sup>.

### Counter-ion exchange:

Prior to photoejection studies and biological testing, each compound was converted to contain Cl<sup>-</sup> counter-ions. The PF<sub>6</sub><sup>-</sup>-salt of compounds **1–4** were converted to Cl<sup>-</sup> salts by dissolving 10–20 mg of product in 1–2 mL methanol. The dissolved product was loaded onto an Amberlite IRA-410 chloride ion exchange column, eluted with methanol, and the solvent was removed *in vacuo*.

#### 4. Photoejection studies.

The half-life of ligand ejection for the complexes **1–4** with the Cl<sup>-</sup> counter-ions were determined in triplicate. The Ru(II) complexes were analyzed in a 96 well plate at a final concentration of 40  $\mu$ M and a path length of 0.5 cm. Scans were taken at set time points for 240 minutes. The normalized change in extinction coefficient was plotted versus time and fit to a mono exponential equation using Prism software.

Quantum yields were determined as has been described previously,<sup>10</sup> with some modification, and different approaches were compared and contrasted. In all cases, the light source was a 470 nm LED array from Elixia. The photon flux of the lamp was determined both by ferrioxalate actinometry and by using a power meter. The procedures are described in detail in Section 7.

**Table S3:** Half-lives of second ligand ejection for **2–4** determined under different buffer conditions

Compound	Sodium phosphate buffer pH 7.4	Potassium phosphate buffer pH 6	Glycine buffer pH 4	Hydrochloric acid-potassium chloride buffer pH 2
<b>2</b>	34.83	20.46	18.73	20.5
<b>3</b>	11.83	6.44	8.15	5.92
<b>4</b>	6.57	3.74	3.11	3.97

#### 5. DNA damage assay.

Ru(II) complexes were serially diluted 1:2 to give final concentrations of 0, 7.8, 15.6, 31.3, 62.5, 125, 250, and 500  $\mu$ M of compound with 40  $\mu$ g/mL of pUC19 plasmid in 10 mM phosphate buffer pH 7.4 in a 96 well plate. Dark control samples were removed prior to light exposure. The samples were irradiate for one hour, aliquots were removed and incubated in the dark overnight. DNA loading dye was added to the samples prior to gel electrophoresis.

Control samples were generated to discriminate between single strand and double strand breaks in the compound-plasmid reactions. To induce single strand breaks, 40  $\mu$ g/mL of pUC19 in 10 mM phosphate buffer, pH 7.4, was mixed with 5  $\mu$ M [Cu(OP)<sub>2</sub>]<sup>2+</sup> and the reaction was initiated upon the addition of 1 mM DTT and 1 mM H<sub>2</sub>O<sub>2</sub>. The reaction was allowed to proceed at room temperature for 30 minutes. For the induction of double strand breaks in pUC19 the restriction enzyme, EcoRI, was used according to the manufacturer's instructions, using 40  $\mu$ g/mL of plasmid. The reaction was allowed to proceed for 90 min at 37 °C and then stored at -20 °C.

Samples with pUC19 plasmid were resolved on a 1% agarose gel in Tris-acetate (TA) buffer, with 0.3  $\mu$ g of plasmid loaded per lane. The samples were run for 90 min at 100 mV followed by staining the gel with a solution of 500 ng/mL ethidium bromide in TA buffer for 40 min. The gels were then destained in TA buffer for 30 min and digitally imaged with the BioRad ChemiDoc System.

## 6. Additional Figures.

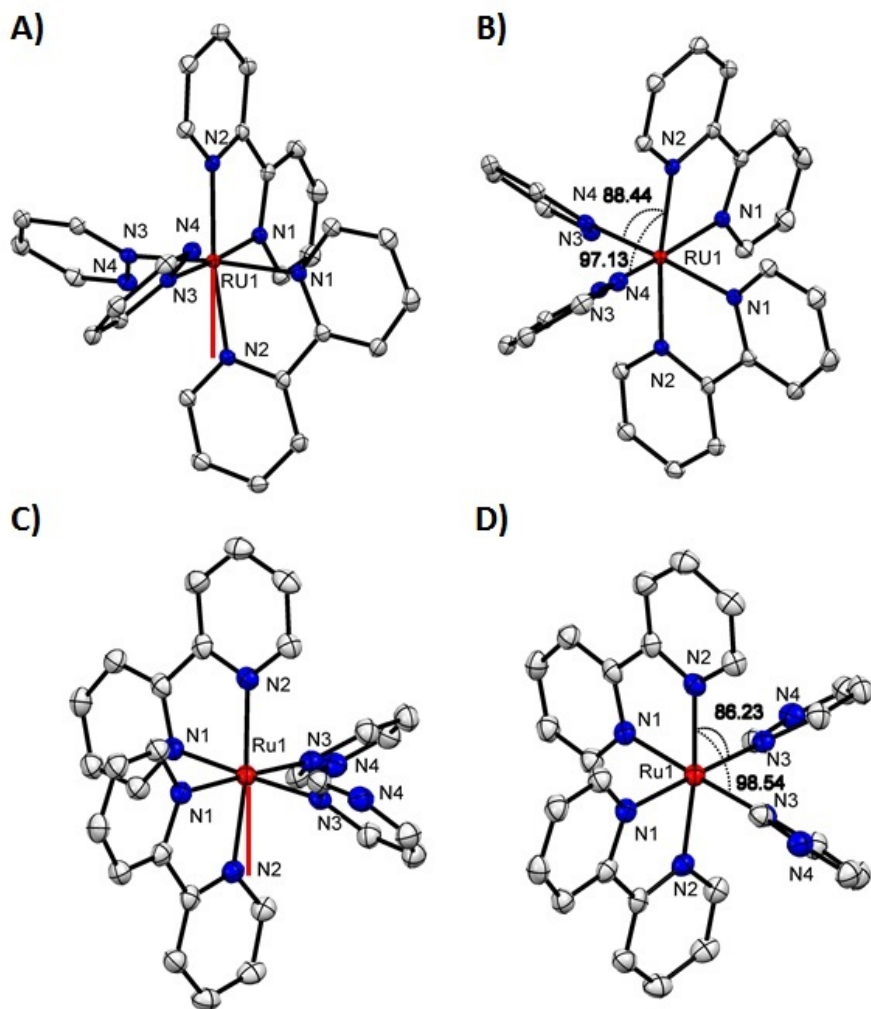


**Figure S1.** Ellipsoid plot of ruthenium complexes  $\Delta$ -2 (A and B) and  $\Delta$ -3 (C and D) at 50% probability with H atoms omitted for clarity. A) and C) - side views highlighting the distortion of the bpy ligands; B) and D) - side views highlighting the bends of the diazines.

**Table S4.** Selected bond lengths (Å) and bond angles (°) of **2** and **3** in comparison with **1**.<sup>11</sup>

	<b>1</b>		<b>2</b>	<b>3</b>
<b>Bond Lengths (Å)</b>				
Ru-N1	2.13(2)	Ru-N1	2.0654(16)	2.064(3)
Ru-N2	2.04(3)	Ru-N2	2.0693(17)	2.070(3)
Ru-N5	2.06(3)	Ru-N3	2.0783(16)	2.108(3)
Ru-N3	2.01(2)	Ru-N1*	2.0654(16)	2.064(3)
Ru-N4	1.99(2)	Ru-N2*	2.0693(17)	2.070(3)
Ru-N6	2.13(2)	Ru-N3*	2.0782(16)	2.108(3)
<b>Bond Angles (°)</b>				
N1-Ru-N3	88(1)	N1-Ru-N1*	90.50(9)	89.12(14)
N1-Ru-N4	94(1)	N1-Ru-N2*	95.68(6)	95.96(10)
N1-Ru-N2	85(1)	N1-Ru-N2	78.60(7)	79.18(10)
N1-Ru-N6	90(1)	N1-Ru-N3*	88.65(7)	90.12(10)
N1-Ru-N5	176(1)	N1-Ru-N3	175.54(6)	177.51(10)
N2-Ru-N6	86(1)	N2-Ru-N3*	88.44(6)	86.22(10)
N2-Ru-N5	91(1)	N2-Ru-N3	97.13(6)	98.54(10)
N4-Ru-N2	175(1)	N2*-Ru-N2	171.96(9)	173.26(14)
N3-Ru-N2	98(1)	N1*-Ru-N2	95.68(6)	95.96(10)
N3-Ru-N4	77(1)	N1*-Ru-N2*	78.59(7)	79.19(10)
N3-Ru-N5	92(1)	N1*-Ru-N3	88.65(7)	90.12(10)
N3-Ru-N6	176(1)	N1*-Ru-N3*	175.54(6)	177.51(10)
N4-Ru-N5	90(1)	N2*-Ru-N3	88.44(6)	86.22(10)
N4-Ru-N6	99(1)	N2*-Ru-N3*	97.13(6)	98.54(10)
N5-Ru-N6	90(1)	N3-Ru-N3*	92.53(9)	90.74(14)

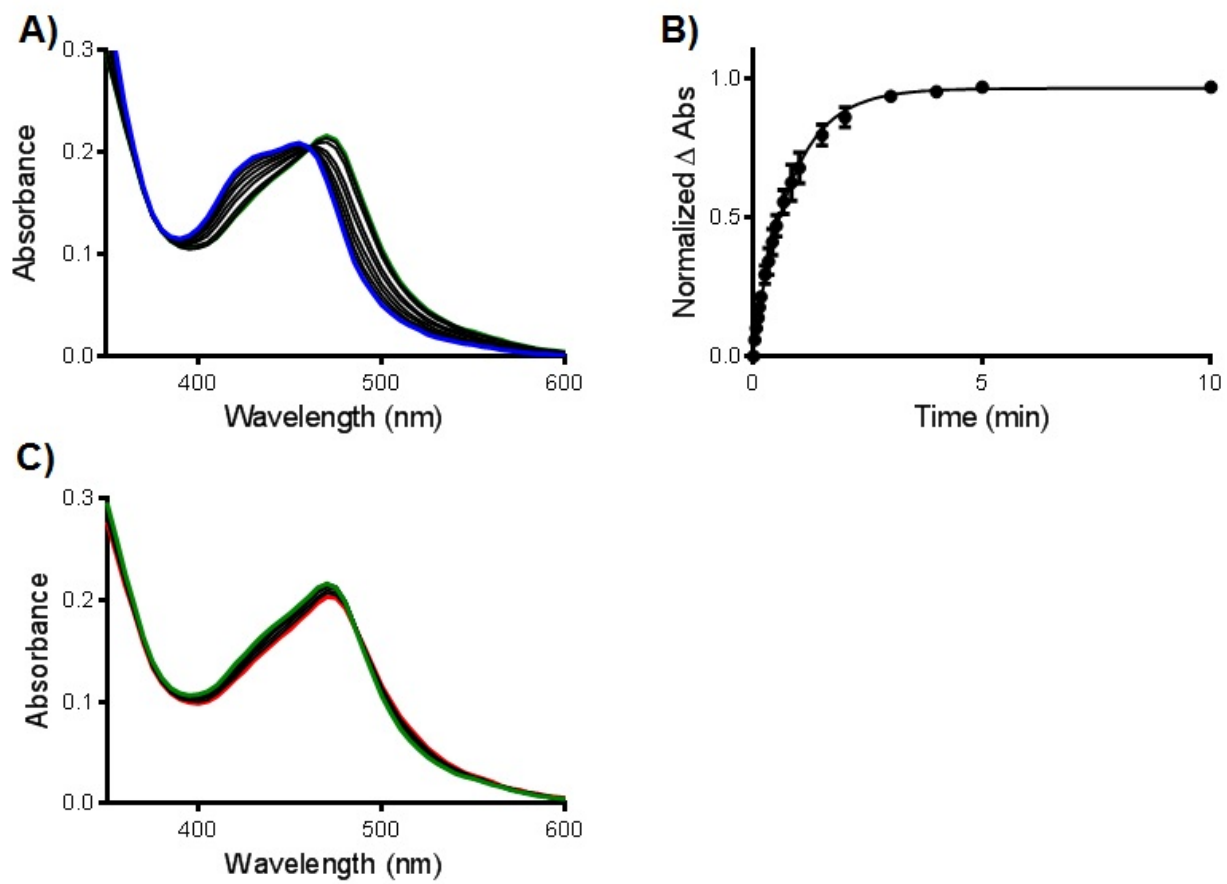


**Figure S2.** Photoejection of 50  $\mu$ M **1** in water for 0–240 min irradiation indicating a one phase process. (A) Time course from 0 (blue) to 5 (green) min. (B) The photoejection kinetics for **1**, with complete ejection of one pyridine ligand in less than 5 min. (C) Time course from 5–240 (red) min followed by UV/vis absorption.

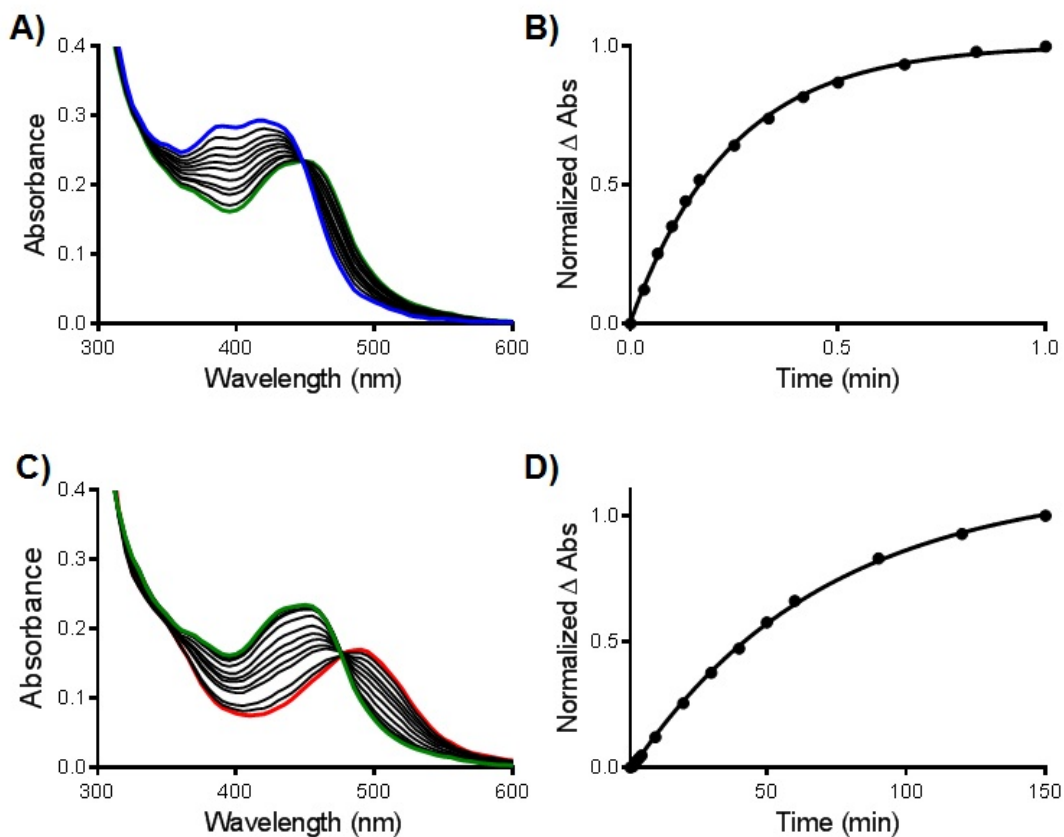


**Figure S3.** Photoejection of 50  $\mu\text{M}$  **2** in water for 0–240 min irradiation indicating a two phase process. (A) Time course from 0 (blue) to 1 (green) min; C) time course from 1–150 (red) min, orange line corresponds to 120 min, followed by UV/vis absorption. The photoejection kinetics for **2**, with complete reaction of first (B) and second (D) pyridazine ligand ejection in less than 1 min and 150 min, respectively.

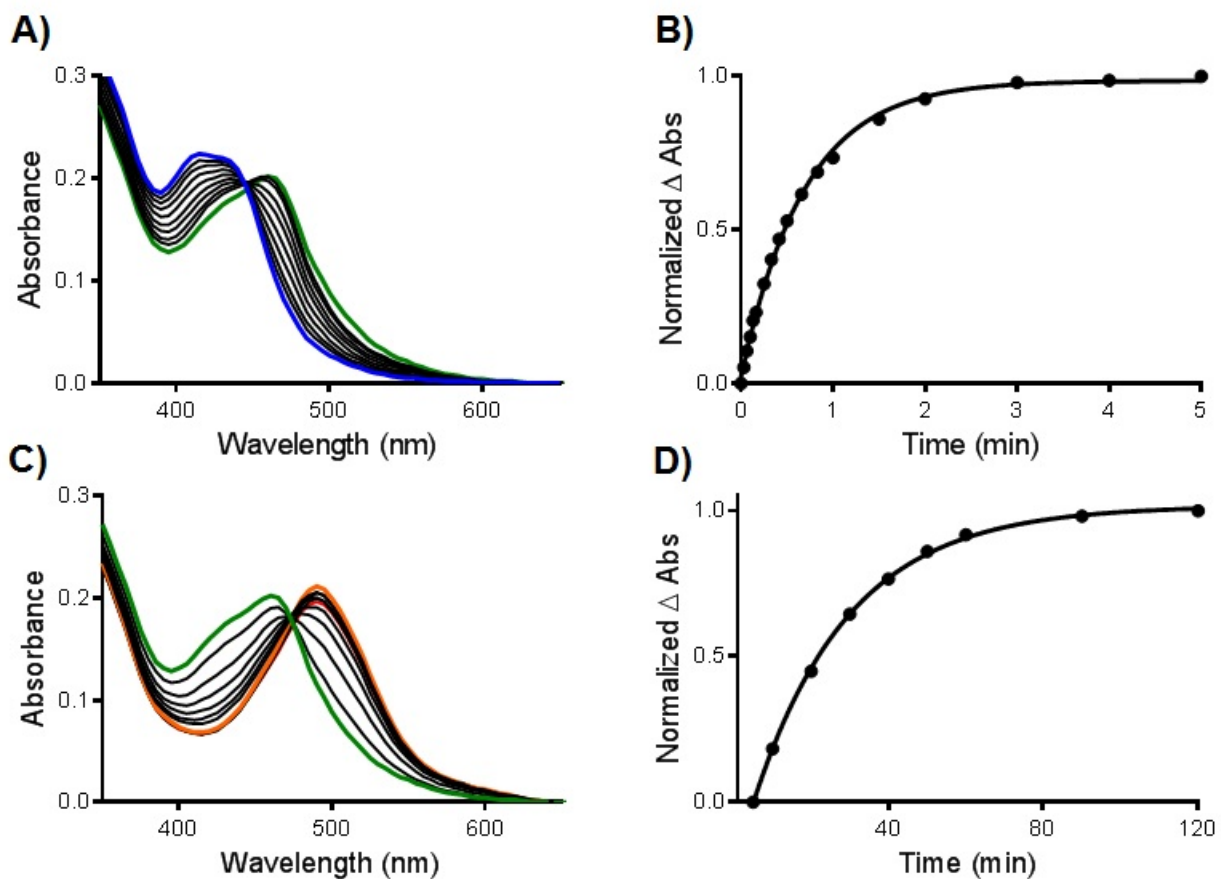


**Figure S4.** Photoejection of 50  $\mu\text{M}$  **3** in water for 0–240 min irradiation indicating a two phase process. (A) Time course from 0 (blue) to 5 (green) min; C) time course from 5–240 (red) min, orange line corresponds to 120 min, followed by UV/vis absorption. The photoejection kinetics for **3**, with complete reaction of first (B) and second (D) pyrimidine ligand ejection in less than 5 min and 120 min, respectively.

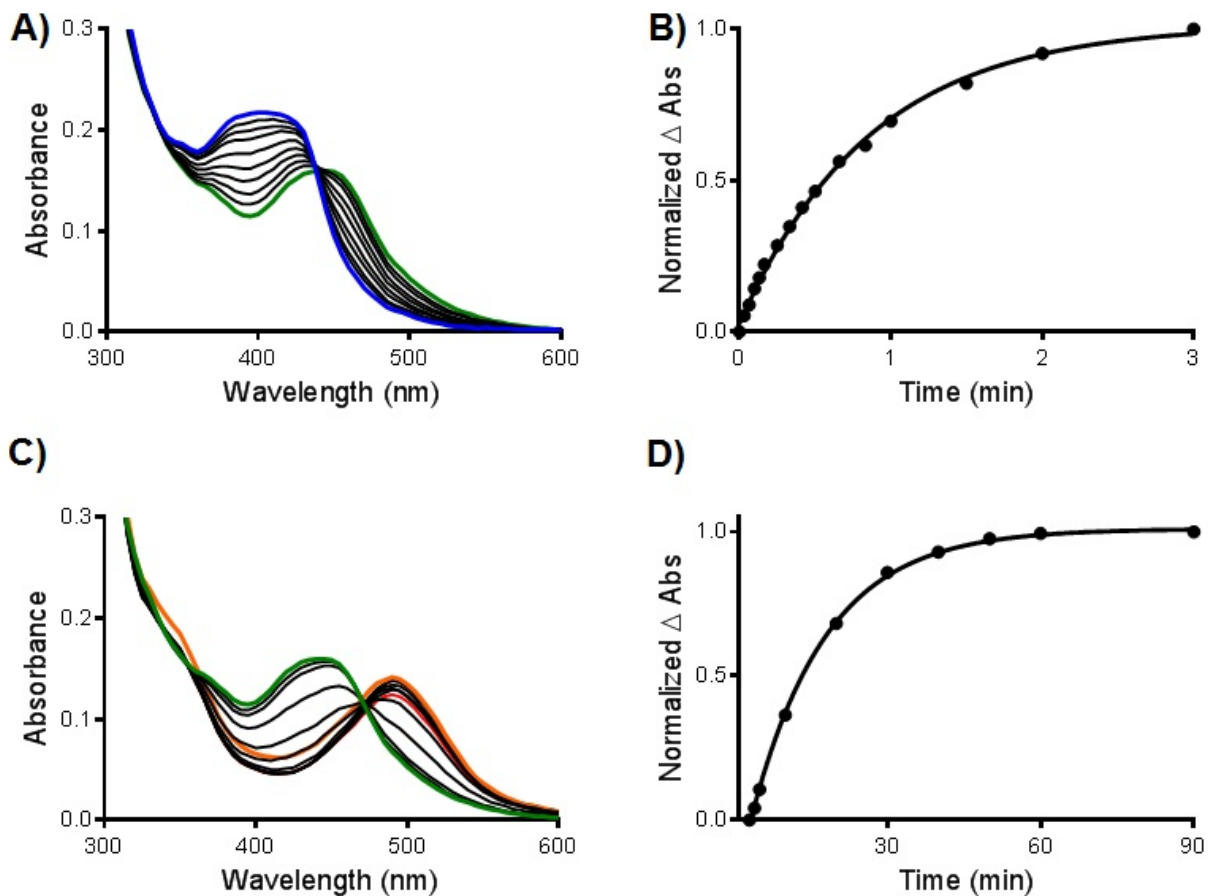


**Figure S5.** Photoejection of 50  $\mu\text{M}$  4 in water for 0–240 min irradiation indicating a two phase process. (A) Time course from 0 (blue) to 3 (green) min; C) time course from 3–240 (red) min, orange line corresponds to 90 min, followed by UV/vis absorption. The photoejection kinetics for 4, with complete reaction of first (B) and second (D) pyrazine ligand ejection in less than 3 min and 90 min, respectively.

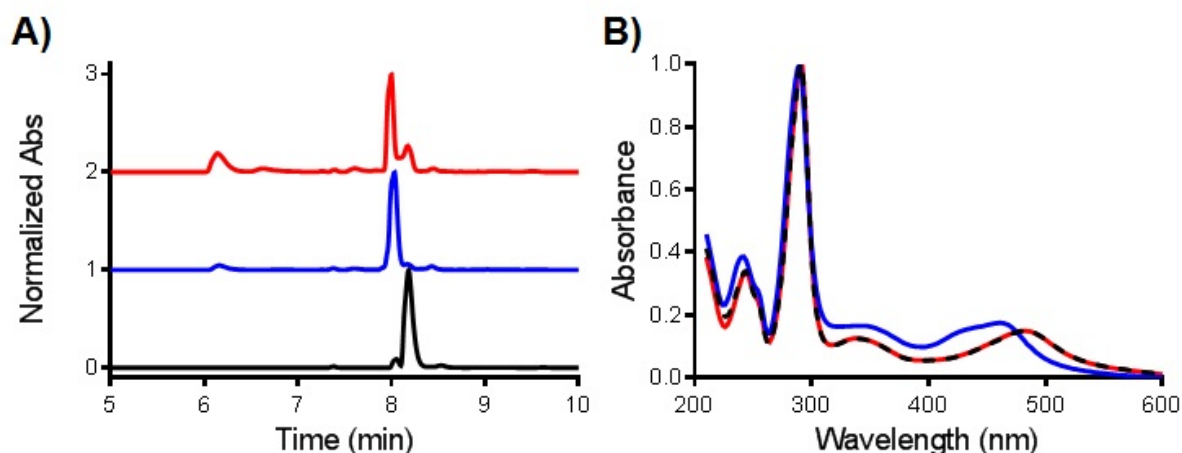


**Figure S6.** Determination of photoejection products by HPLC for compound **3**. A) HPLC chromatogram of **3** before irradiation (black line) and after irradiation for 5 min (blue line) and 120 min (red line). (B) Absorption profile of Ru(II) products for compound **3** after ejection of first (blue line, 5 min irradiation, retention time = 8.03 min), the second pyrimidine ligand (red line, 120 min irradiation, retention time = 7.99 min), and compound **5** after 15 min irradiation (black dash line, retention time = 7.87 min). The photochemical product of **5** and the final product of **3** is  $[\text{Ru}(\text{bpy})_2(\text{H}_2\text{O})_2]^{2+}$ .

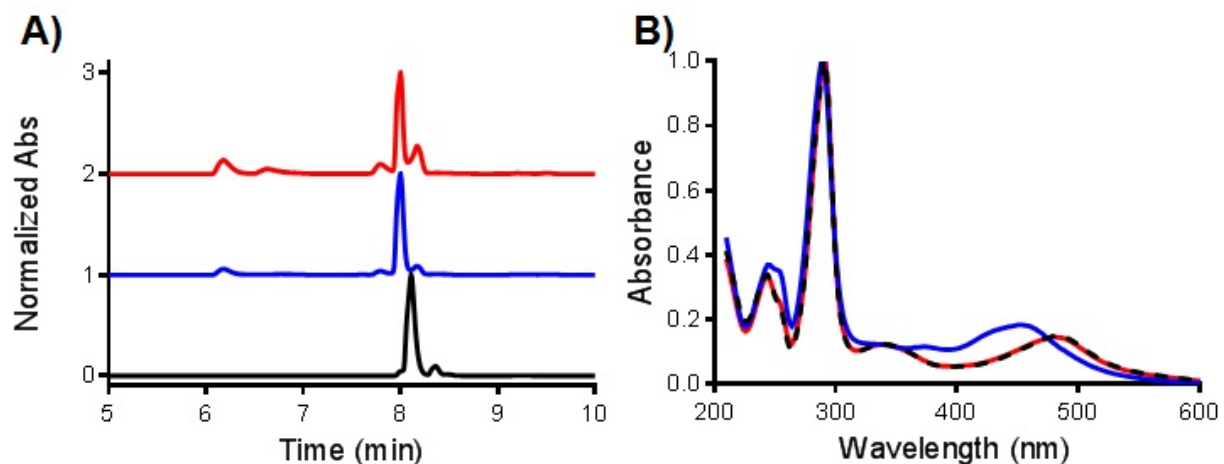


**Figure S7.** Determination of photoejection products by HPLC for compound **4**. A) HPLC chromatogram of **4** before irradiation (black line) and after irradiation for 5 min (blue line) and 120 min (red line). (B) Absorption profile of Ru(II) products for compound **4** after ejection of first (blue line, 5 min irradiation, retention time = 8.08 min), the second pyrazine ligand (red line, 120 min irradiation, retention time = 7.99 min), and compound **5** after 15 min irradiation (black dash line, retention time = 7.87 min). The photochemical product of **5** and the final product of **4** is  $[\text{Ru}(\text{bpy})_2(\text{H}_2\text{O})_2]^{2+}$ .

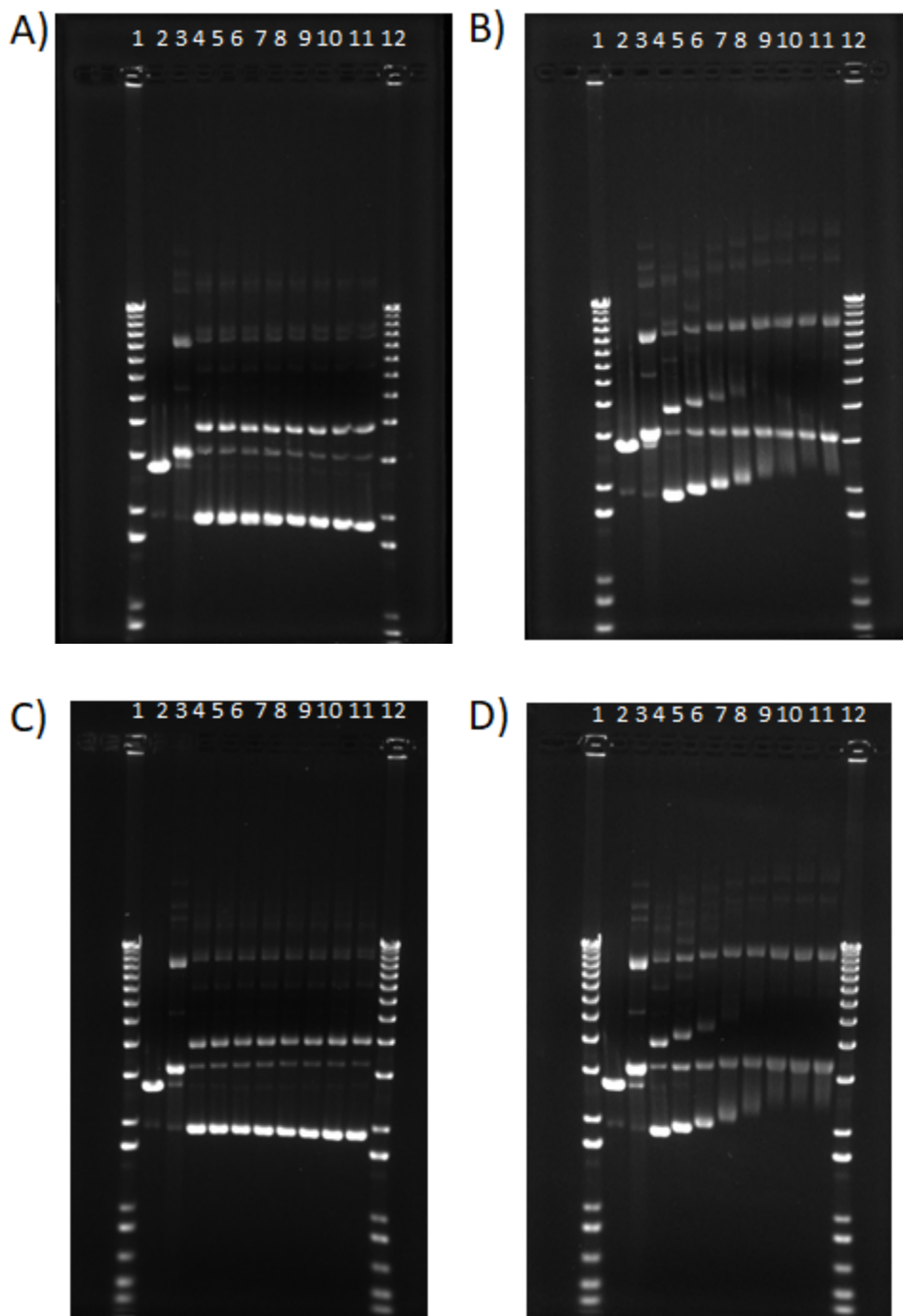


**Figure S8.** Agarose gel electrophoresis showing the dose response without (A, C) and after 1 hour irradiation (B, D) of **1** (A, B) and **2** (C, D) incubated with 40  $\mu\text{g}/\text{mL}$  pUC19 DNA. Lanes 1 and 12, DNA ladder; lane 2, EcoRI; lane 3,  $\text{Cu}(\text{OP})_2$ ; lane 4–11, 0–500  $\mu\text{M}$ . EcoRI and  $\text{Cu}(\text{OP})_2$  are controls for linear and relaxed circle DNA. There is no DNA remaining in the wells.

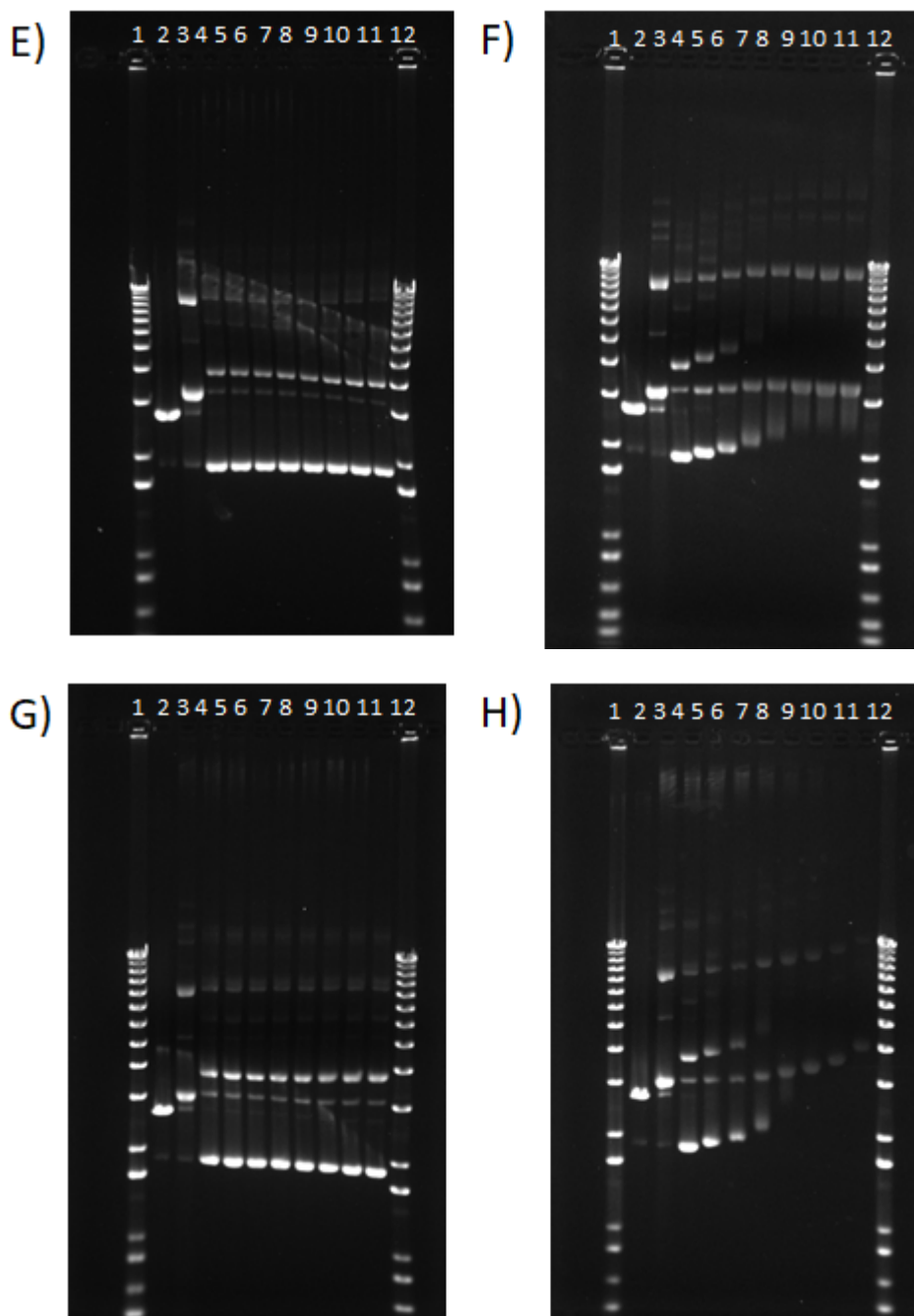


**Figure S8 (continuation).** Agarose gel electrophoresis showing the dose response without (E, G) and after 1 hour irradiation (F, H) of **3** (E, F) and **4** (G, H) incubated with 40  $\mu\text{g}/\text{mL}$  pUC19 DNA. Lanes 1 and 12, DNA ladder; lane 2, EcoRI; lane 3,  $\text{Cu}(\text{OP})_2$ ; lane 4–11, 0–500  $\mu\text{M}$ . EcoRI and  $\text{Cu}(\text{OP})_2$  are controls for linear and relaxed circle DNA. There is no DNA remaining in the wells.

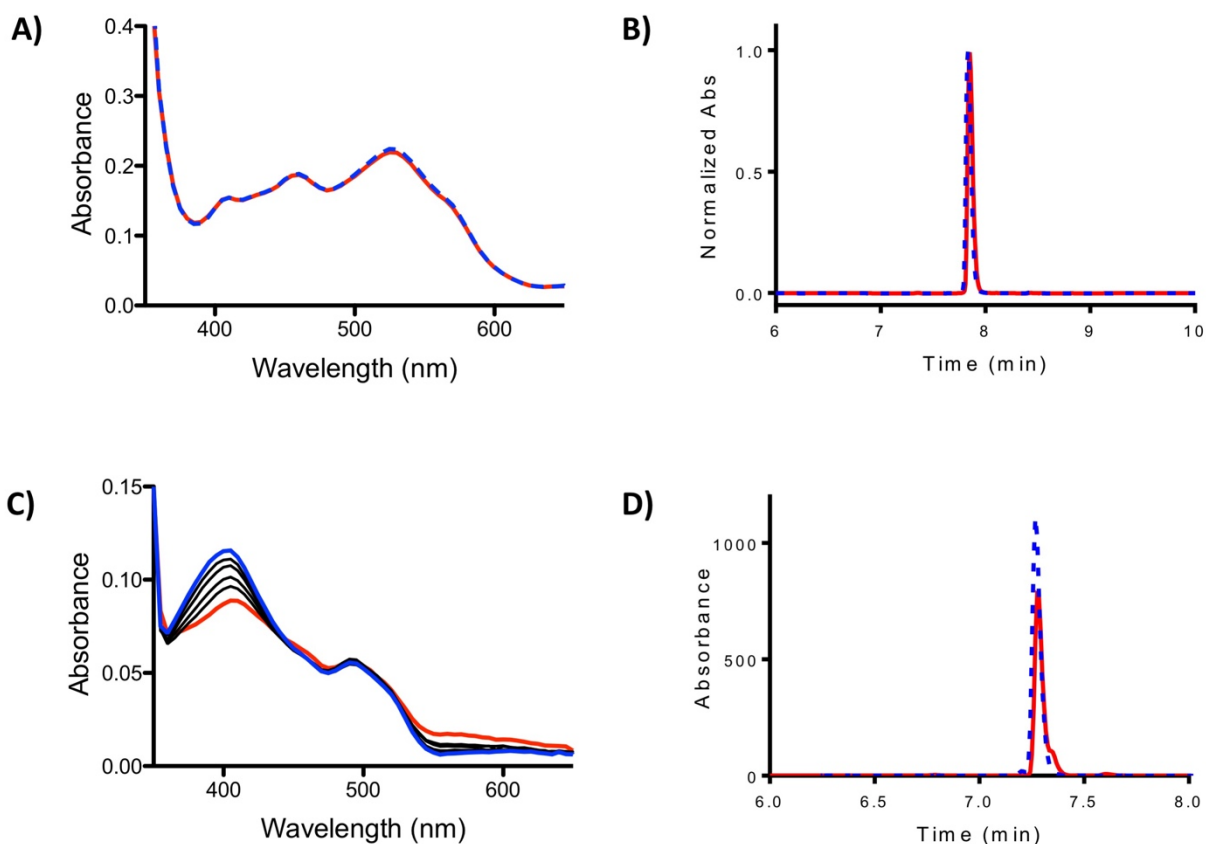


**Figure S9.** Photoejection of **6** (A, B) and **7** (C, D) in water for 0-540 min irradiation monitored by UV/Vis absorbance and HPLC. UV/Vis spectra of **6** (A) and **7** (C) in water for 0-540 min irradiation indicates no photoejection for compound **6** and slow ligand release for **7**. Determination of photoejection products by HPLC for compounds **6** (B) and **7** (D): HPLC chromatograms before irradiation (blue dash line) and after irradiation for 540 min (red line).

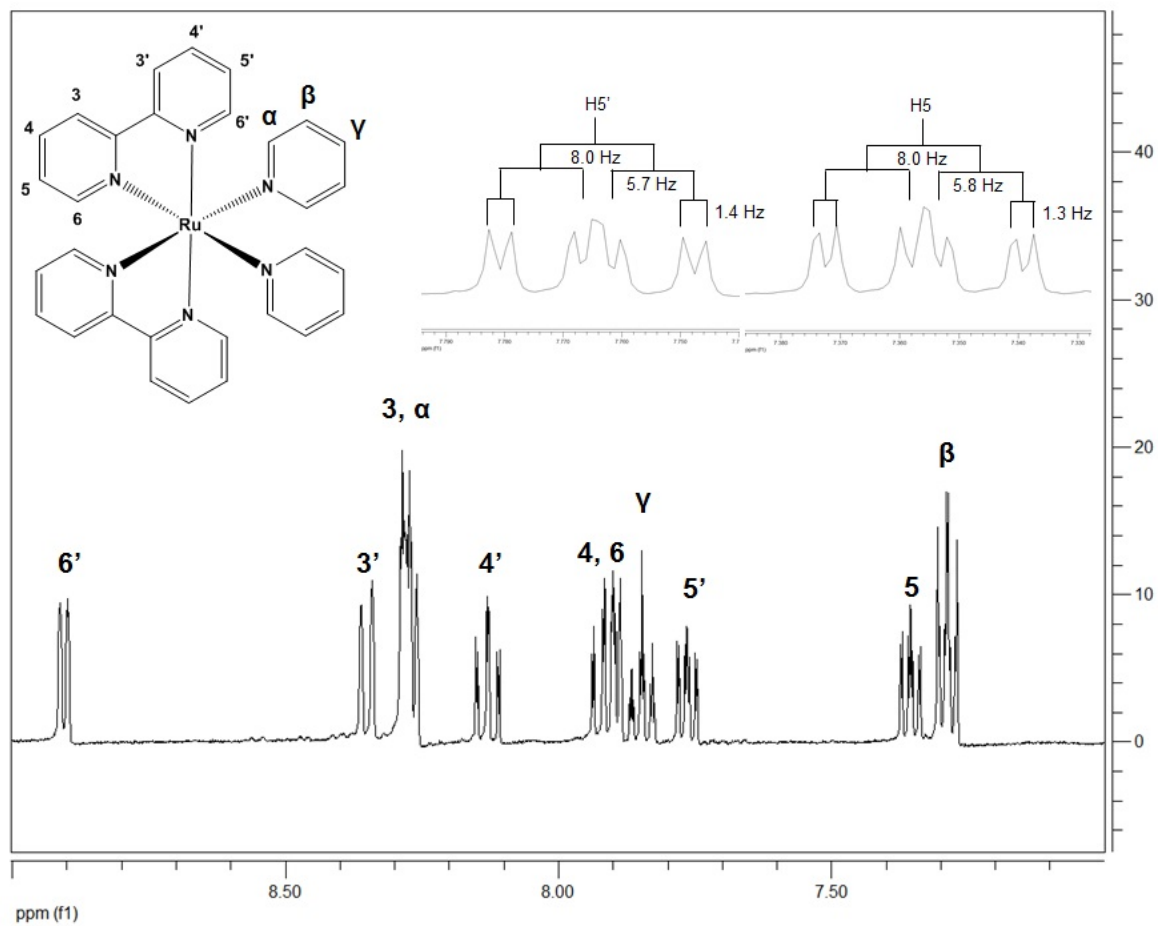


**Figure S10.**  $^1\text{H}$  NMR of **1** in  $\text{CD}_3\text{CN}$ .

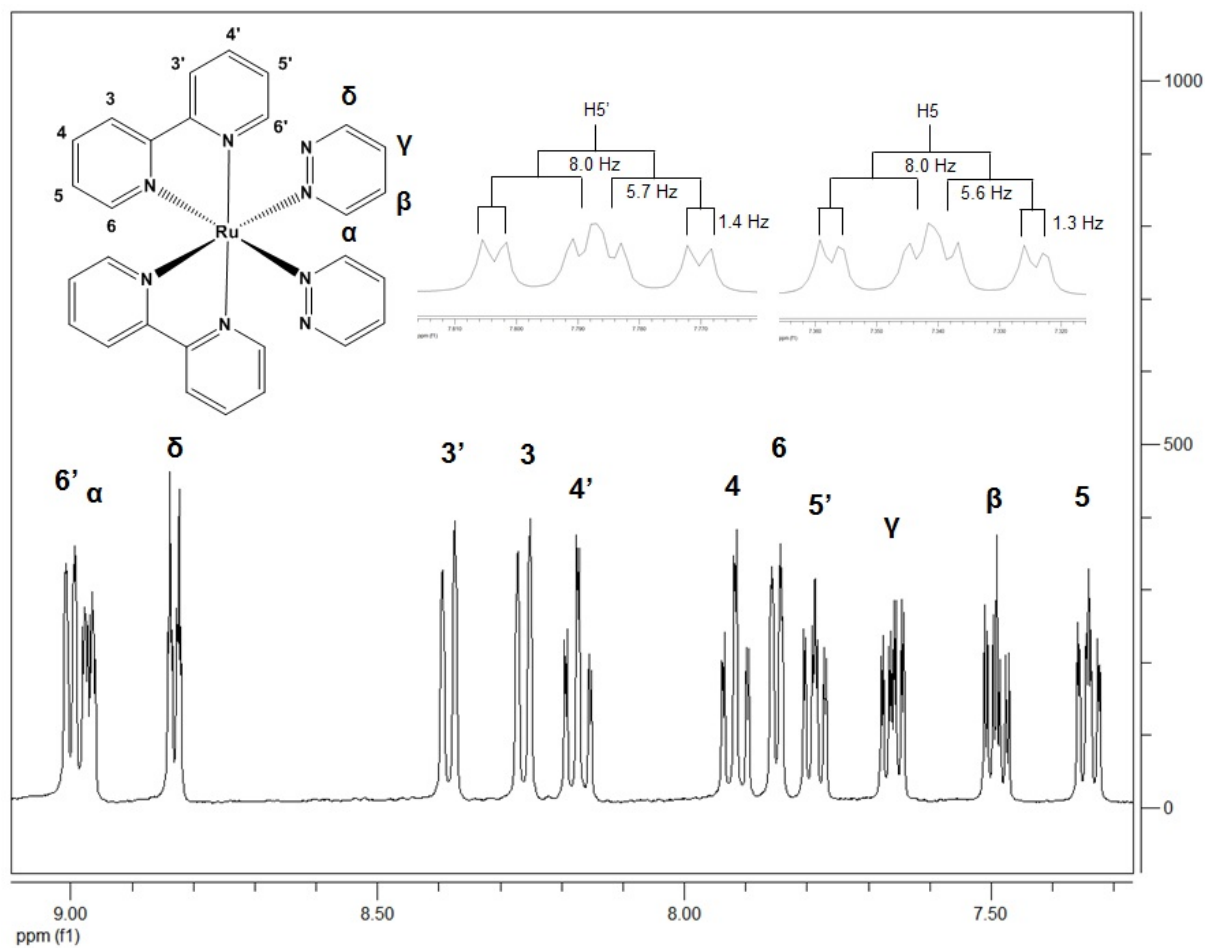


**Figure S11.**  $^1\text{H}$  NMR of **2** in  $\text{CD}_3\text{CN}$ .

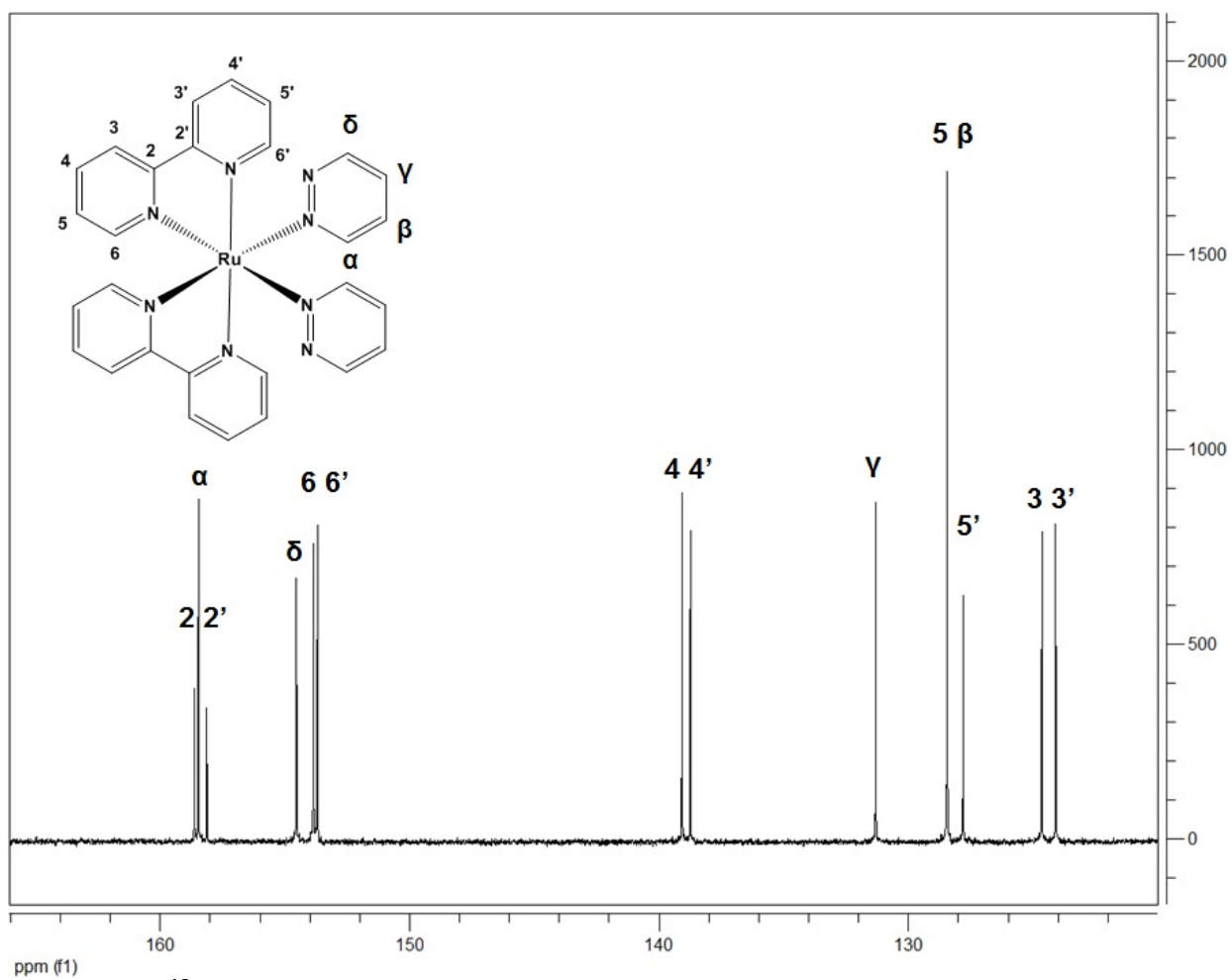


**Figure S12.**  $^{13}\text{C}$  NMR of **2** in  $\text{CD}_3\text{CN}$ .

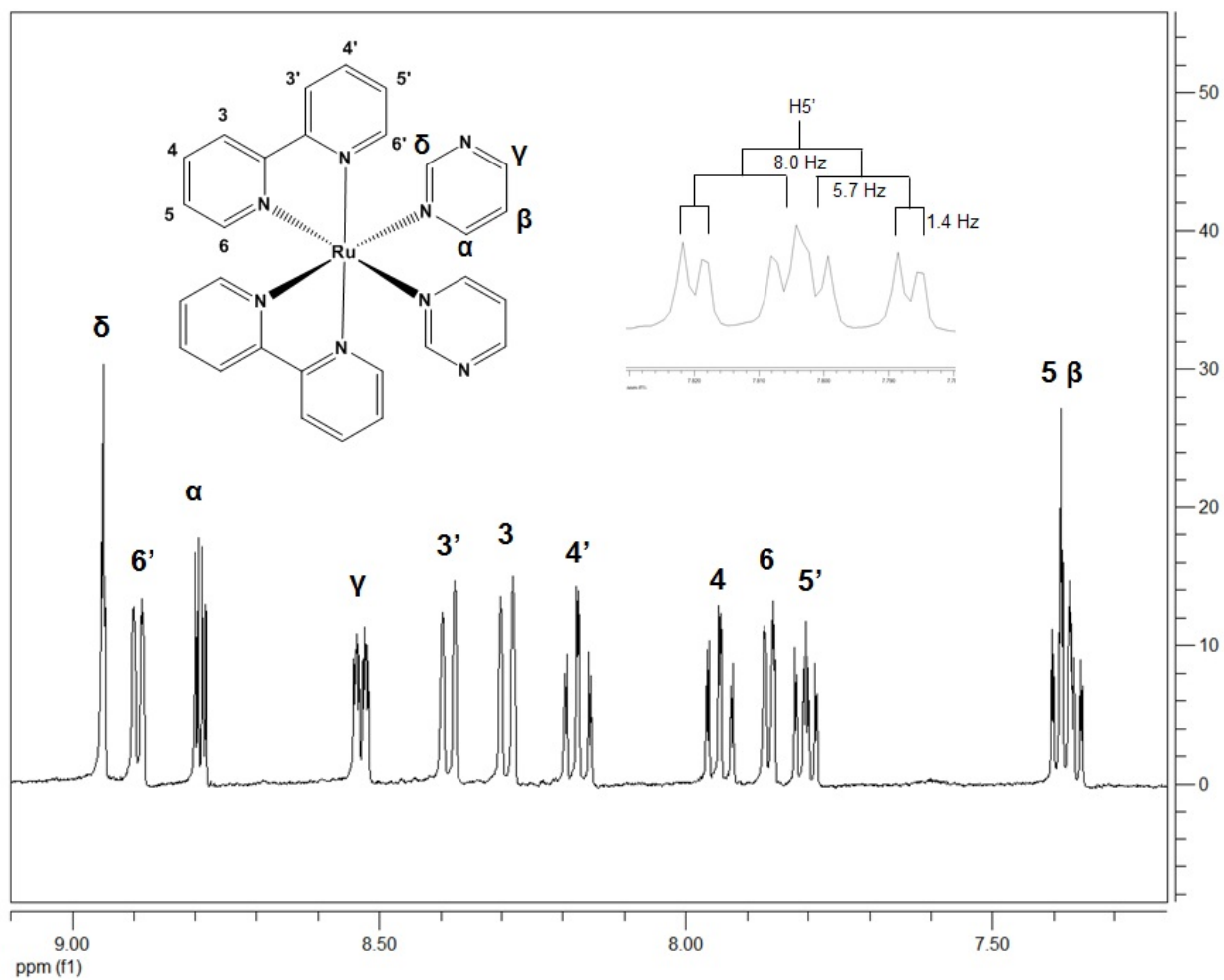


**Figure S13.**  $^1\text{H}$  NMR of **3** in  $\text{CD}_3\text{CN}$ .

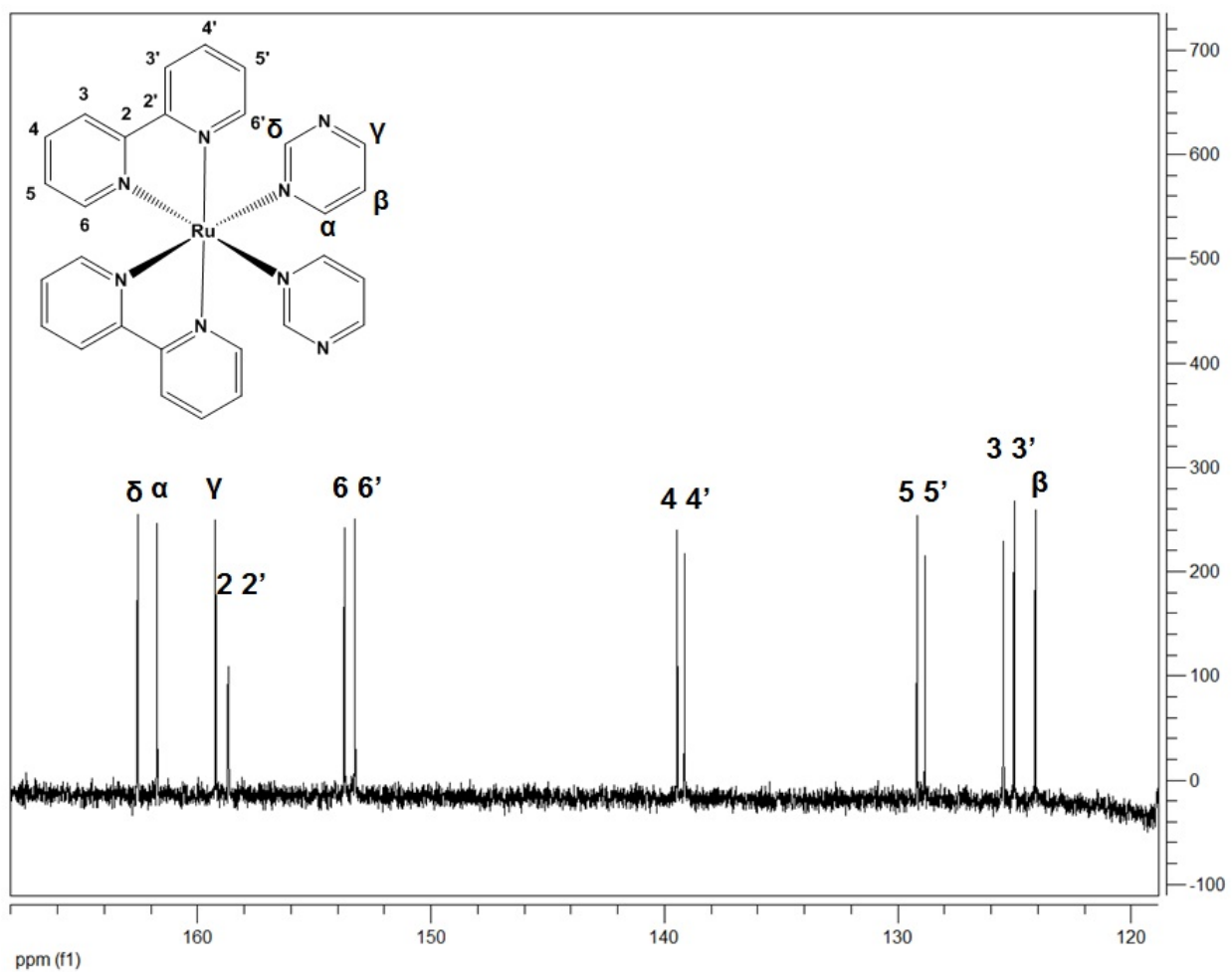


**Figure S14.**  $^{13}\text{C}$  NMR of **3** in  $\text{CD}_3\text{CN}$ .

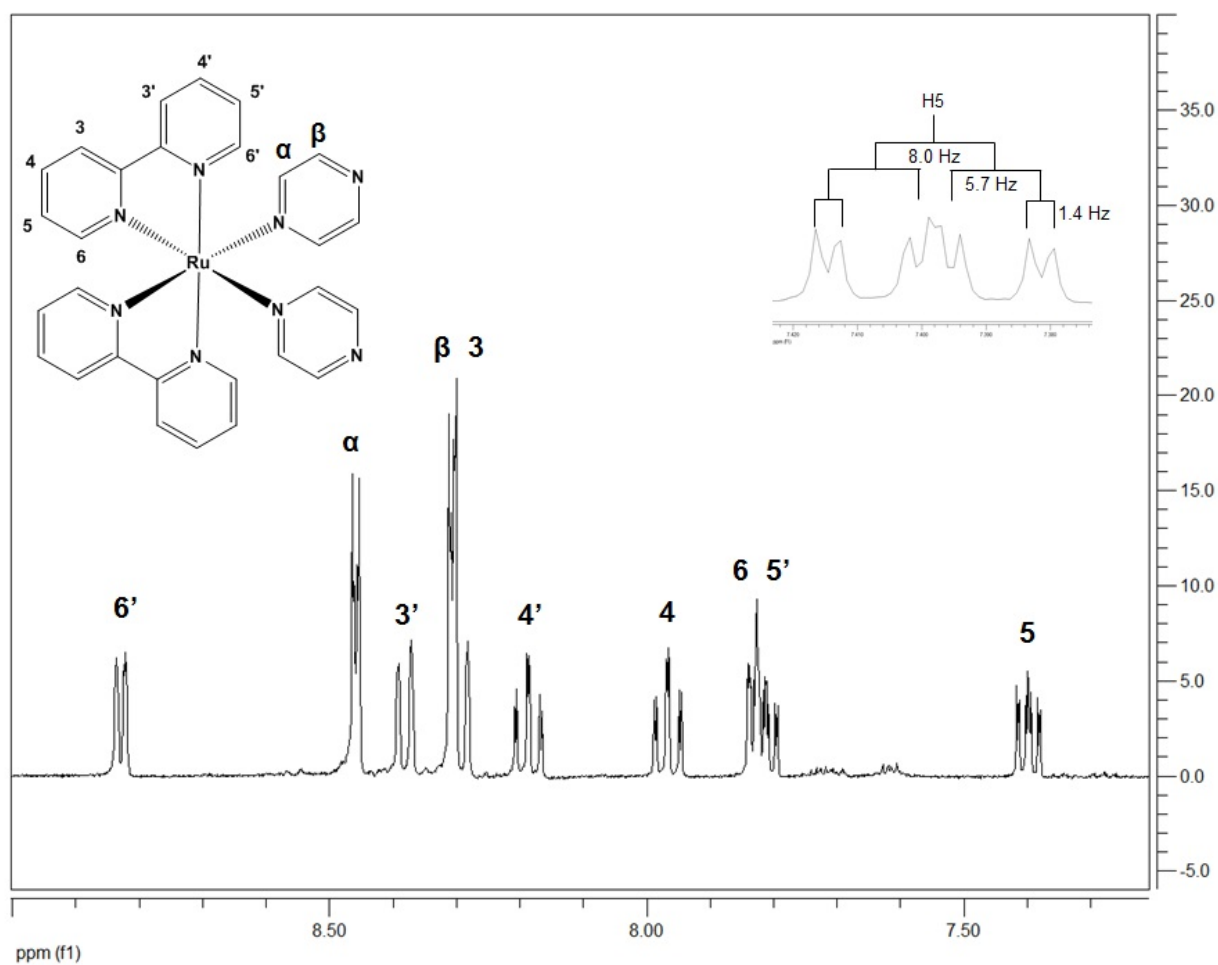


**Figure S15.**  $^1\text{H}$  NMR of **4** in  $\text{CD}_3\text{CN}$ .

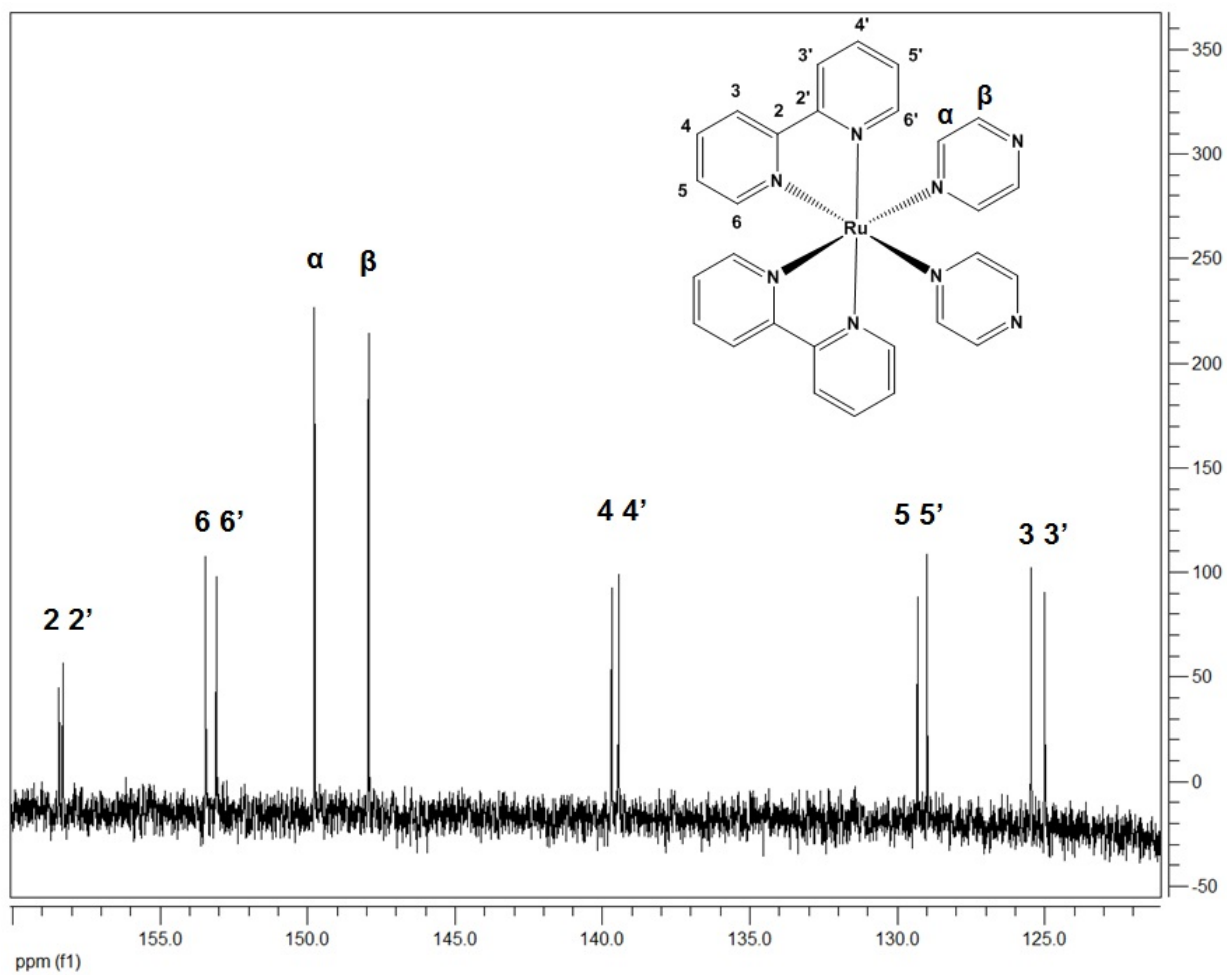


**Figure S16.**  $^{13}\text{C}$  NMR of **4** in  $\text{CD}_3\text{CN}$ .

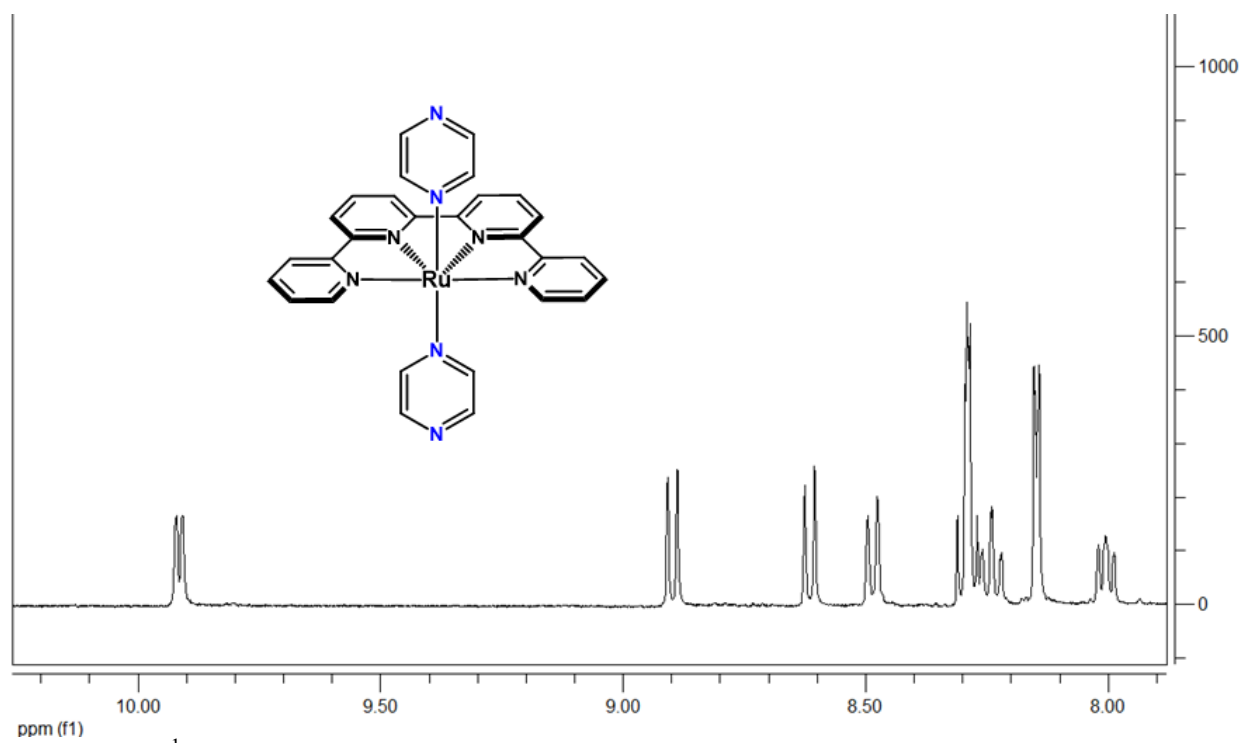


**Figure S17.**  $^1\text{H}$  NMR of 7 in DMSO.

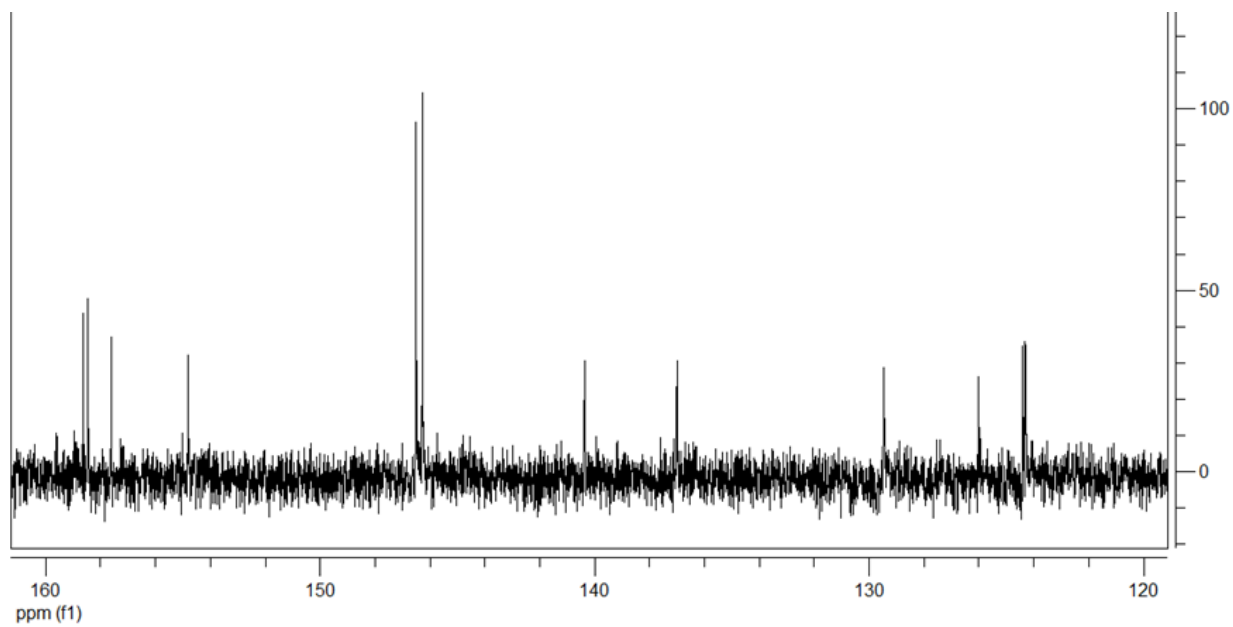


**Figure S18.**  $^{13}\text{C}$  NMR of 7 in DMSO.

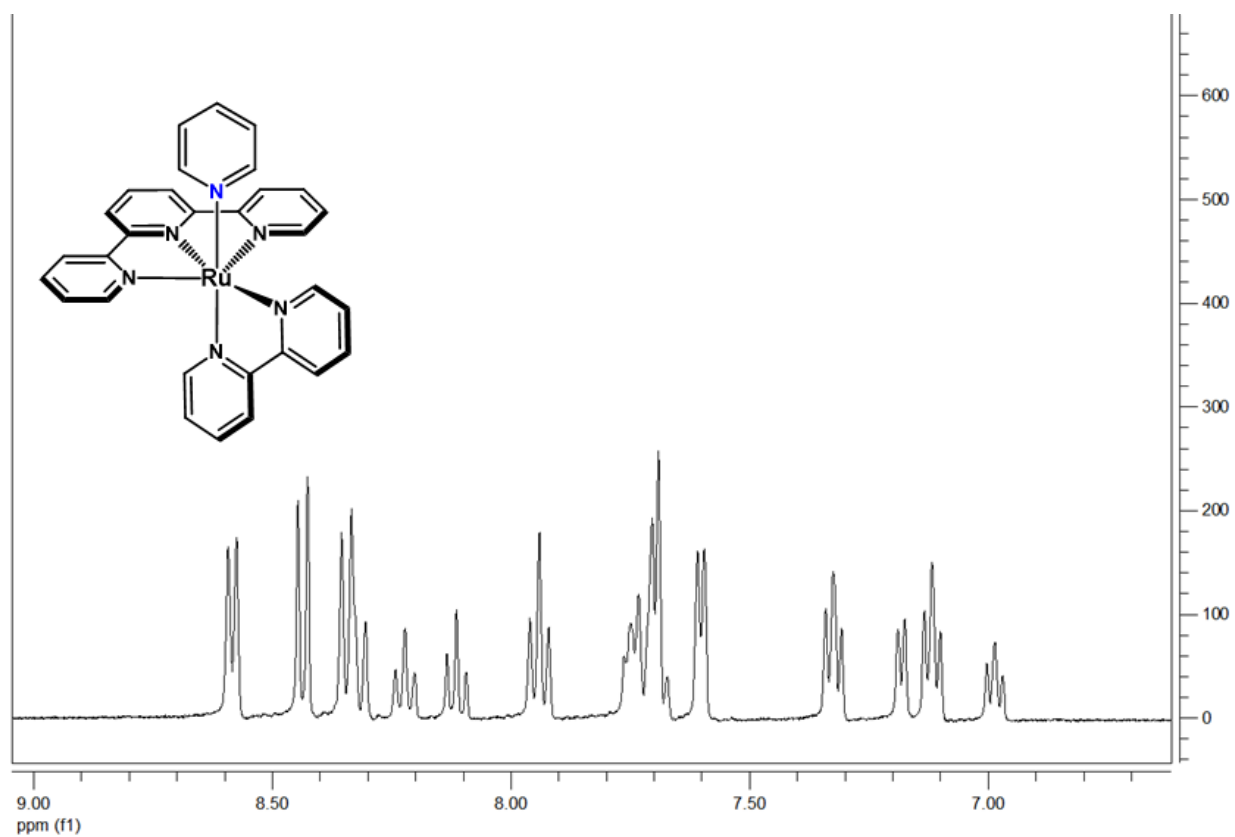


**Figure S19.**  $^1\text{H}$  NMR of **8** in  $\text{CD}_3\text{CN}$ .

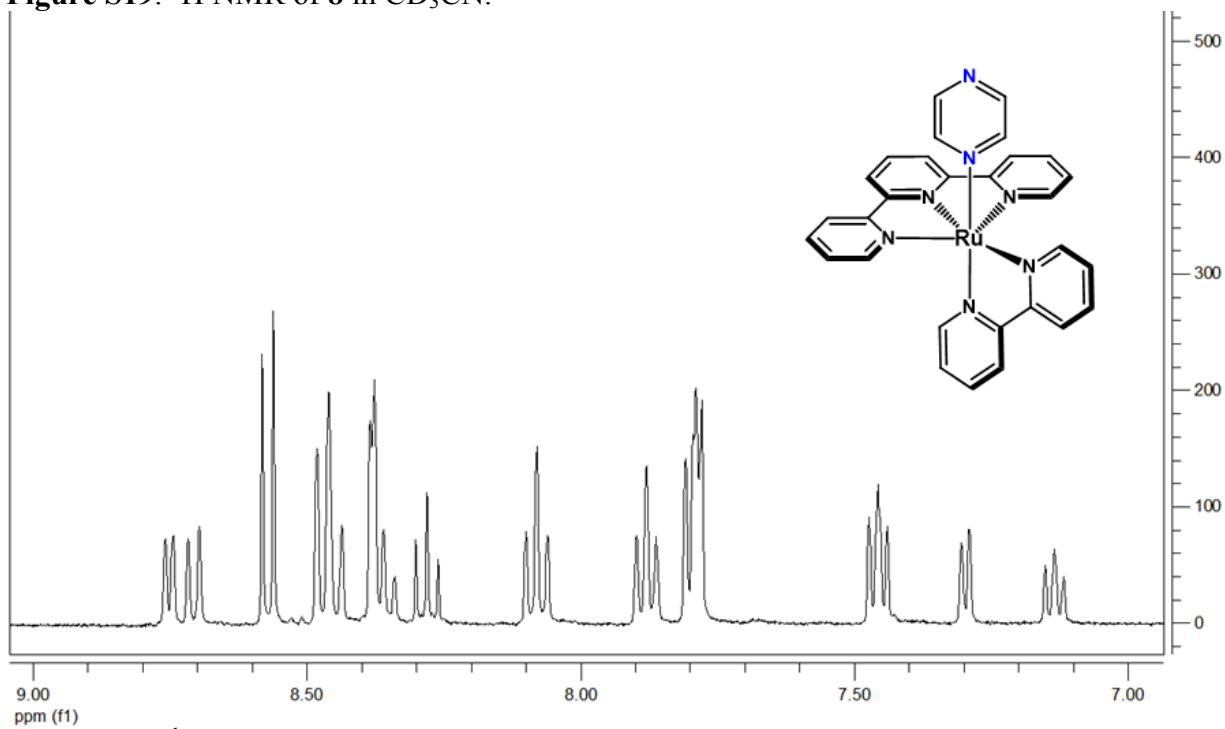


**Figure S20.**  $^1\text{H}$  NMR of **9** in  $\text{CD}_3\text{CN}$ .

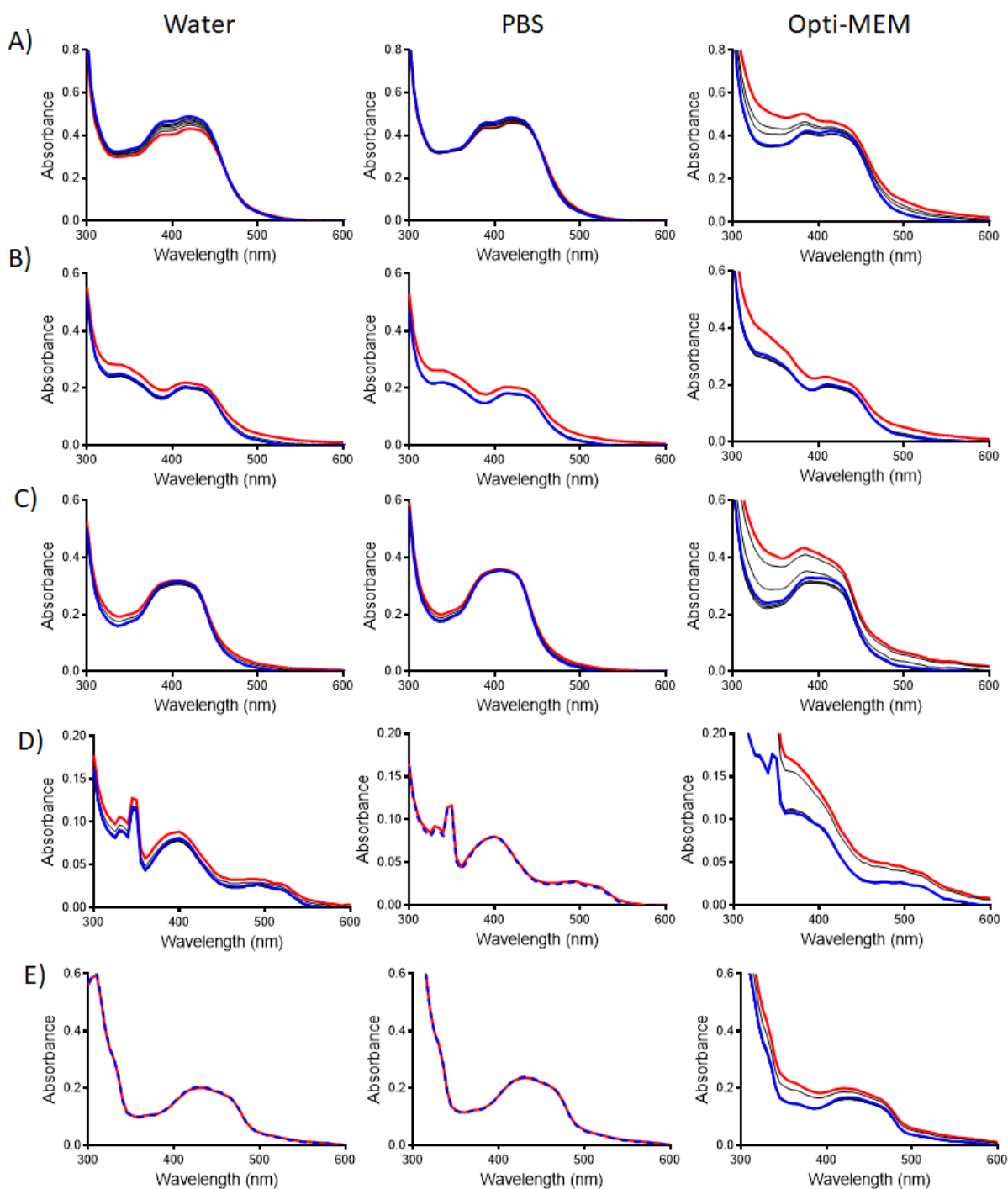


**Figure S21.** Stability of complexes **2** (A), **3** (B), **4** (C), **7** (D), and **9** (E) in water (left), potassium buffer solution, pH = 7.4 (middle) and Opti-MEM (right) at 37 °C in the dark over the course of 0 (blue line) to 72 h (red line). Compound **2** demonstrates 88% remaining unchanged after 72 h in water, and 95% in buffer solution. The increase in absorbance at the last time point can be explained by the evaporation of the solvent from the 96-well plate.

## 7. Detailed methods for determination of quantum yields

### Procedure for Ferrioxilate Actinometry Method I:

- 1) Solution 1: A solution of potassium ferrioxalate (0.15 M, prepared by dissolving 0.7369 g potassium ferrioxalate in 10 mL 0.05 M sulfuric acid) was used as an actinometer according to C. G. Hatchard and C. A. Parker *Proceedings of the Royal Society of London. Series A, Mathematical and Physical Sciences* Vol. 235, No. 1203 (Jun. 12, 1956), pp. 518-536. In this publication, the fraction of light absorbed was 0.85, and the quantum yield at 468 nm was reported as 0.92 in Table 4.
- 2) Solution 2: A solution of 1% 1,10-phenanthroline was prepared in buffer (1.125 sodium acetate trihydrate, 50 mg 1,10-phenanthroline, 0.14 mL (0.2646 g) of H<sub>2</sub>SO<sub>4</sub> in water, diluted to 5 mL).
- 3) Solution 1 (0.2 mL) was added into each well of a 96 well plate, and irradiated for set times. At each time point, 10 μL aliquots of Solution 1, 30 μL of Solution 2, and 160 μL of H<sub>2</sub>O were combined to determine the absorbance of Fe<sup>2+</sup> complex at 510 nm. This complex forms as a result of photolysis of the ferrioxalate.
- 4) The photon flux of light source was determined by two different approaches, as shown below, with two experimental replicates.

**Approach 1:**

Photon flux calculated from values in Table.

**Table S5.** Experiment 1.

Time (sec)	Abs, 510 nm	$\Delta$ Abs 510 nm	C(Fe <sup>2+</sup> )	Moles	Moles irradiated	Abs, 470 nm	F	Photon flux
		$\Delta A = A_t - A_0$	$C(Fe^{2+}) = \Delta A / (\epsilon * l)$	$mol = C * V3$	$mol(irr) = mol * V1/V2$			$q = mol(irr) / (\phi * t * F)$
0	0.078	0	0	0	0	0.26	0.45	-
5	0.108	0.03	5.45455E-06	1.09091E-09	2.18182E-08			1.05294E-08
10	0.158	0.08	1.45455E-05	2.90909E-09	5.81818E-08			1.40393E-08
15	0.205	0.127	2.30909E-05	4.61818E-09	9.23636E-08			1.48582E-08
20	0.268	0.19	3.45455E-05	6.90909E-09	1.38182E-07			1.66716E-08
30	0.413	0.335	6.09091E-05	1.21818E-08	2.43636E-07			1.95965E-08
40	0.509	0.431	7.83636E-05	1.56727E-08	3.13455E-07			1.89091E-08
50	0.599	0.521	9.47273E-05	1.89455E-08	3.78909E-07			1.82861E-08
60	0.662	0.584	0.000106182	2.12364E-08	4.24727E-07			1.70811E-08
								<b>1.62464E-08</b>

**Table S6.** Experiment 2.

Time (sec)	Abs, 510 nm	$\Delta$ Abs 510 nm	C(Fe <sup>2+</sup> )	Moles	Moles irradiated	Abs, 470 nm	F	Photon flux
		$\Delta A = A_t - A_0$	$C(Fe^{2+}) = \Delta A / (\epsilon * l)$	$mol = C * V3$	$mol(irr) = mol * V1/V2$			$q = mol(irr) / (\phi * t * F)$
0	0.095	0	0	0	0	0.26	0.45	-
5	0.109	0.014	2.54545E-06	5.09E-10	1.01818E-08			4.91374E-09
10	0.179	0.084	1.52727E-05	3.05E-09	6.10909E-08			1.47412E-08
15	0.216	0.121	0.000022	4.4E-09	0.000000088			1.41562E-08
20	0.262	0.167	3.03636E-05	6.07E-09	1.21455E-07			1.46535E-08
30	0.398	0.303	5.50909E-05	1.1E-08	2.20364E-07			1.77246E-08
40	0.507	0.412	7.49091E-05	1.5E-08	2.99636E-07			1.80755E-08
50	0.562	0.467	8.49091E-05	1.7E-08	3.39636E-07			1.63908E-08
60	0.642	0.547	9.94545E-05	1.99E-08	3.97818E-07			1.59989E-08
								<b>1.45818E-08</b>

## Approach 2:

The change in absorbance of  $[\text{Fe}^{2+}]$  at 510 nm was plotted against irradiation time.

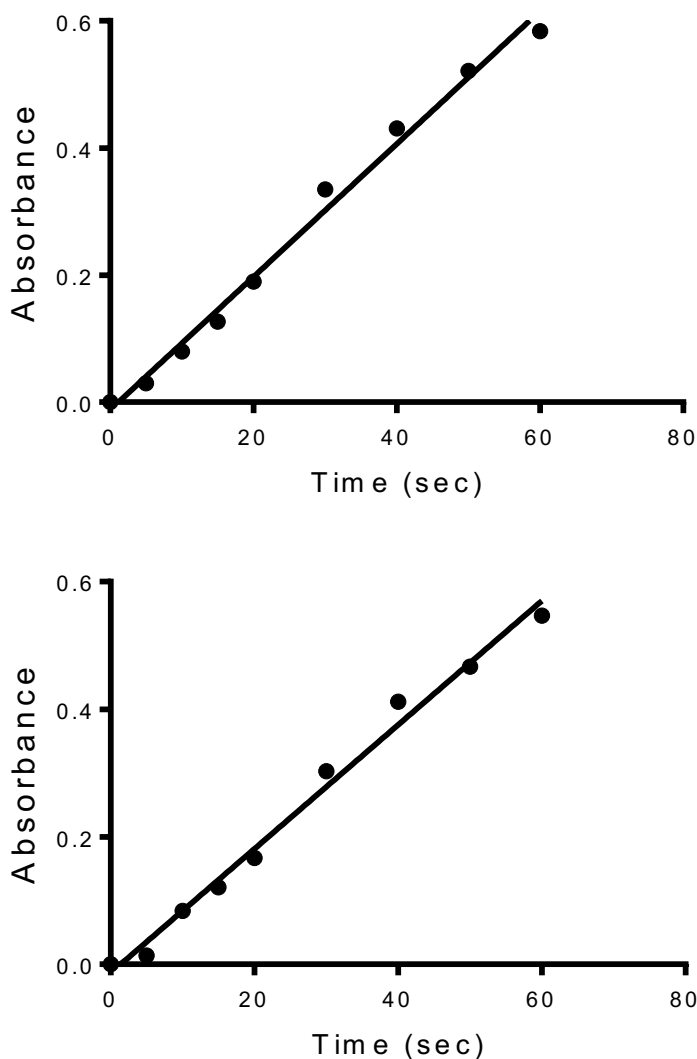


**Figure S22.** Linear regression of absorbance vs. time for  $[\text{Fe}(\text{phen})_3]^{2+}$  complex formation.

The slope corresponds to the  $dA/dt$  value to solve for the photon flux ( $q$ ):

$$q = \frac{dA}{dt} * \frac{V1}{\epsilon * l} * \frac{V3}{V2 * \phi * F}$$

Where  $q$  is photon flux (einstein/s),  $dA/dt$  is slope,  $V1$  – volume of irradiated actinometer (0.15 M, 200  $\mu\text{L}$ ),  $V2$  is the aliquot of actinometer taken to determine the concentration of  $[\text{Fe}(\text{phen})_3]^{2+}$  (10  $\mu\text{L}$ ),  $V3$  is the volume of the solution measured after complexation (200  $\mu\text{L}$ ),  $\epsilon$  is the extinction coefficient of  $[\text{Fe}(\text{phen})_3]^{2+}$  (11,000),<sup>12</sup>  $l$  is the path length (0.5 cm in the 96 well plate),  $\phi$  is the

quantum yield of actinometer at 468 nm  $(0.92)^{13}$  and  $F = 1-1/10^{A_{(470)}}$  is the photon absorption probability for the actinometer in the plate reader well (which was calculated to be equal to 0.45 at 470 nm).

The photon flux was also calculated based on Digital Handheld Optical Power and Energy Meter Console (PM100D, ThorLabs).

**Table S7.** Photon flux of light source obtained by different calculations

Experiment	Slope	Power	Photon Flux ( $q$ , Einstein/s)
Actinometer 1	0.009721	-	1.71E-08
Actinometer 2	0.01046	-	1.83E-08
Power Meter	-	8.3 mW	3.26E-08

Finally, the photon flux was calculated by monitoring the disappearance of the ferrioxalate. This is a faster approach that requires less material.

#### **Procedure for Potassium Ferrioxalate Actinometry Method II**

- 1) A solution was prepared by dissolving 2 mg potassium ferrioxalate in 3 mL 0.05 M sulfuric acid.
- 2) Aliquots of 200  $\mu$ L were dispensed in each well in a 96-well plate. Absorbance spectra were taken at  $t = 0$ .
- 3) The sample was irradiated and absorbance readings taken at set time points.
- 4) The absorbance at 390 nm was plotted against time.

**Table S8.** Ferrioxalate absorbance values at various time points.

Plate reader file	Time (sec)	A(390)	A(390)	A(390)	Average Absorbance
		Sample 1	Sample 2	Sample 3	
1278	0	0.247	0.247	0.248	0.247333
1281	10	0.244	0.244	0.246	0.244667
1284	30	0.236	0.235	0.237	0.236
1286	50	0.23	0.23	0.231	0.230333
1287	70	0.224	0.222	0.224	0.223333
1288	90	0.219	0.218	0.22	0.219
1289	120	0.211	0.21	0.212	0.211
1290	180	0.194	0.193	0.196	0.194333
1291	240	0.18	0.178	0.179	0.179

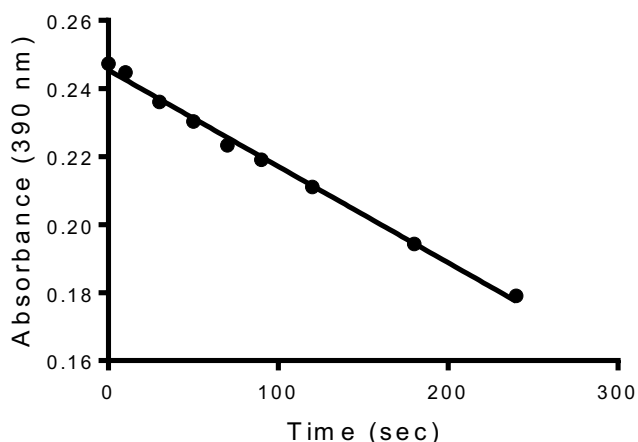


**Figure S23.** Linear regression of absorbance vs. time for disappearance of ferrioxalate.

- 5) The slope corresponds to the  $dA/dt$  value used to solve for the photon flux,  $q$ , giving a value of  $5.66236\text{E-}09$  einstein/s.

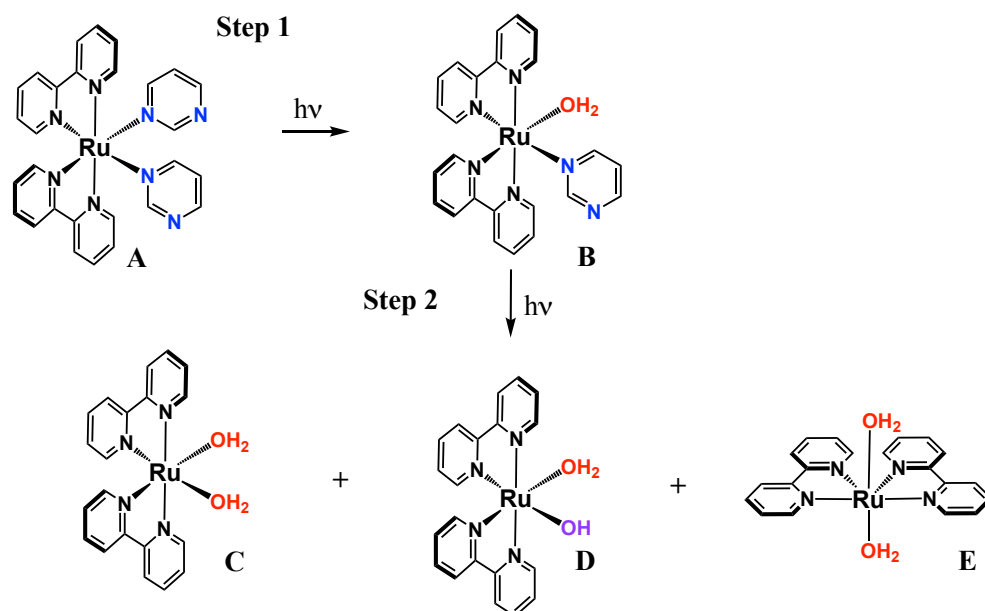
$$q = \frac{dA}{dt} * \frac{V}{\epsilon * l * \phi * F}$$

Where  $q$  is photon flux (einstein/s),  $dA/dt$  is slope,  $V$  – volume of irradiated actinometer (200  $\mu\text{L}$ ),  $\epsilon$  is the extinction coefficient of potassium ferrioxalate ( $312 \text{ mol}^{-1}\text{dm}^3\text{cm}^{-1}$ ),  $l$  is the path length (0.5 cm in well plate),  $\phi$  is the quantum yield of actinometer at 468 nm (0.92) and  $F = 1 - 1/10^{A_{(470)}}$  is the photon absorption probability for actinometer in plate reader well ( $A_{(470)} = 0.03$ ;  $F = 0.0667$ ).

In order to evaluate the accuracy of the photon flux measurement,  $cis\text{-}[\text{Ru}(\text{bpy})_2(\text{MeCN})_2]^{2+}$  (the  $\text{Cl}^-$  salt) was used as a control. Different values for  $\phi_{\text{PS}}$  have been reported; for example,  $\phi_{\text{PS}} = 0.44$  for the release of the first ligand in one report,<sup>14</sup> which matches a previously reported value in 1 M  $\text{H}_2\text{SO}_4$ ,<sup>15</sup>  $\phi_{\text{PS}} = 0.21$  in another,<sup>16</sup> but it is not explicitly clear if this is for the first or second ligand, or the average of the two photochemical processes. Using the value for  $q$  obtained from ferrioxalate actinometry using Method I, we observed  $\phi_{\text{PS}} = 0.22$  for the release of the first ligand, which matches well with the cited value.<sup>16</sup> For all subsequent quantum yield determinations, we used  $q = 1.77\text{E-}08$  (average of values obtained by Method 1, Approach 2).

### Quantum Yield Determination

The calculation of quantum yields of photosubstitution reactions of Ru(II) complexes based on the change in absorbance ( $\Delta \text{Abs}$ ) at initial time points is widely reported.<sup>17-18</sup> However this approach is not convenient for our compounds, considering the absorption profile of initial complexes and photoproducts overlap, and this is especially complicated for the determination of quantum yields for the second step of the photosubstitution reactions. However, the change in absorbance upon irradiation possessed clear isobestic points for both Steps 1 and 2 (Figures S3-5) of photosubstitution. As a result, the moles of decreasing reactant (for example, “B” in Scheme S1) were determined based on the changes in normalized corrected  $\Delta$  Absorbance (reactant vs. product) over time, which is used in the  $t_{1/2}$  determinations.



**Scheme S1.** Photoproducts of complex **3** generated in water upon irradiation with 470 nm light. The second photoejection step is accompanied by generation of other species (“D” and “E”).<sup>19</sup> Thus, the loss of the intermediate (“B” in this scheme) is monitored rather than the appearance of a single product (“C”).

The photoejection of the monodentate ligands in water was monitored by absorption spectroscopy (Fig. S2–5). Complexes **1–4** and **9** (200  $\mu$ L, 50  $\mu$ M) were irradiated with 470 nm light in 96-well plate. To calculate the photosubstitution quantum yield for Step 1, the average absorbance for the first five time points (0, 2, 4, 6, and 8 seconds) at 470 nm was measured and used for the calculation of the photon absorption probability (F) for each complex. The second step of the photochemical reaction occurred after 1 min. Accordingly, the average absorbance at 470 nm was measured for the five time points after 1 min irradiation (60, 90, 120, 180, 240 seconds) was used for calculation of the photon absorption probability (F) of the intermediate photosubstitution (Step 2) for complexes **2–4**.

**Table S9.** Photon absorption probability for compound **1–4, 9**.

Comp	<b>1</b>	<b>2</b>		<b>3</b>		<b>4</b>		<b>9</b>
Step	1	1	2	1	2	1	2	1
Abs (470)	0.177	0.127	0.193	0.096	0.178	0.051	0.111	0.177
F	0.335	0.254	0.359	0.199	0.336	0.111	0.226	0.335

The quantum yield calculation for complex **3** is described below, based on the UV/Vis spectroscopy. It was further confirmed by HPLC determination.

### Calculation of quantum yield for complex **3** based on UV/Vis.

The corrected change in absorbance ( $\Delta A_{corr}$ ) was calculated for each time point as:

$$\Delta A_{corr} = A_t^{460} - A_t^{415} - (A_0^{460} - A_0^{415})$$

were  $A_t^{460}$  is the MLCT absorbance of photoproduct/intermediate (Step 1) at each time point (t) increasing over time,  $A_t^{415}$  is MLCT absorbance of complex **3** at each time point (t) decreasing over time,  $A_0^{460}$  is the initial MLCT absorbance of photoproduct/intermediate (Step 1), and  $A_0^{415}$  is initial MLCT absorbance for complex **3**.

The normalized corrected change in absorbance has been calculated for each time point as:

$$\text{Normalized } \Delta A_{corr} = 1 - \Delta A_{corr} / \Delta A_{corr}^{max}$$

Where  $\Delta A_{corr}^{max}$  is maximum corrected change in absorbance.

We postulated that the normalized corrected change in absorbance with a value of 1 corresponds to the maximum (initial) moles of complex **3** before irradiation, and employed this to calculate the moles of the starting complex and product at each time point.

The initial moles (*mol*) in the well has been calculated as

$$\text{mol} = A_0^{415} * V / (\epsilon * l)$$

Where  $A_0^{415}$  is initial MLCT absorbance for complex **3**,  $V$  is the aliquot irradiated (200  $\mu$ L),  $\epsilon$  is the extinction coefficient for complex **3**, and  $l$  is the path length (0.5 cm in plate reader well).

The moles of photon absorbed have been calculated as the product of photons irradiated and photon absorption probability (F).

**Table S10.** Parameters used to calculate moles of reactant and photons absorbed at each time point of irradiation for compound **3** (Step 1).

Time, seconds	Photons irradiated, moles	Photons absorbed, moles	$A_t^{415}$	$A_t^{460}$	$\Delta A_{corr}$	Normalized $\Delta A_{corr}$	Moles of $[\text{Ru}(\text{bpy})_2(\text{pym})_2]^{2+}$
0	0	0	0.224286	0.148286	0	1	9.34525E-09
2	3.54E-08	7.04E-09	0.220286	0.152286	0.008	0.930434783	8.69515E-09
4	7.01E-08	1.40E-08	0.21819	0.15519	0.013	0.886956522	8.28883E-09
6	1.06E-07	2.12E-08	0.214667	0.157667	0.019	0.834782609	7.80125E-09
8	1.42E-07	2.82E-08	0.211048	0.160048	0.025	0.782608696	7.31367E-09
10	1.77E-07	3.52E-08	0.210095	0.163095	0.029	0.747826087	6.98862E-09
15	2.66E-07	5.29E-08	0.20419	0.16819	0.04	0.652173913	6.09473E-09
20	3.54E-07	7.05E-08	0.198143	0.173143	0.051	0.556521739	5.20083E-09
25	4.43E-07	8.81E-08	0.194952	0.176952	0.058	0.495652174	4.63199E-09
30	5.31E-07	1.06E-07	0.191143	0.181143	0.066	0.426086957	3.98189E-09
40	7.01E-07	1.40E-07	0.185095	0.186095	0.077	0.330434783	3.088E-09
45	8.85E-07	1.76E-07	0.180952	0.189952	0.085	0.260869565	2.43789E-09
60	1.06E-06	3.57E-07	0.177048	0.193048	0.092	0.2	1.86905E-09
90	1.59E-06	3.17E-07	0.16881	0.19981	0.107	0.069565217	6.50104E-10
120	2.12E-06	4.23E-07	0.162762	0.201762	0.115	0	0

The quantum yield of photolysis was calculated as a slope of the liner regression (the moles of reactant vs. moles of photon absorbed).

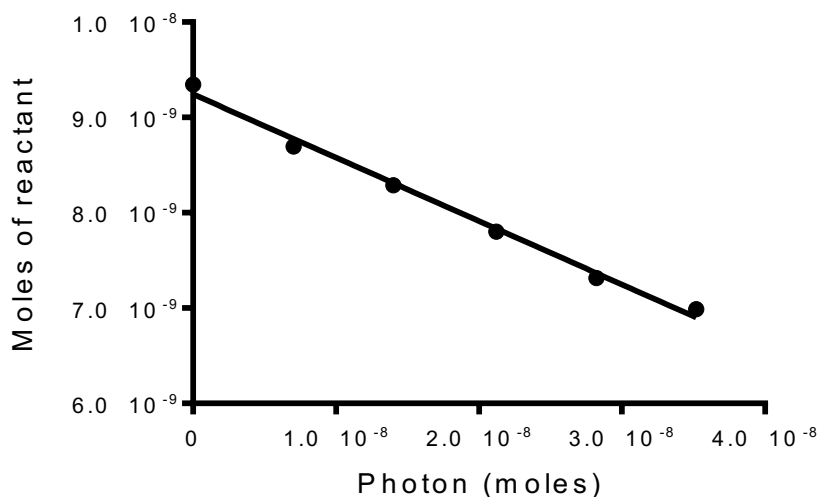


**Figure S24.** Liner regression for moles of reactant vs. moles of photons absorbed for Step 1 (complex 3).

The same approach has been used to calculate the quantum yield for Step 2 of photosubstitution reaction.

**Table S11.** Parameters used to calculate moles of reactant and photons absorbed at each time points of irradiation for compound 3 (Step 2).

Time, seconds	Photons irradiated, moles	Photons absorbed, moles	$A_t^{460}$	$A_t^{490}$	$\Delta A_{corr}$	Normalized $\Delta A_{corr}$	Moles of $[\text{Ru}(\text{bpy})_2(\text{pym})(\text{H}_2\text{O})]^{2+}$
60	1.06E-06	3.57E-07	0.193048	0.087048	0	0	9.34525E-09
90	1.59E-06	3.17E-07	0.19981	0.09581	0.002	0.010582011	9.24636E-09
120	2.12E-06	4.23E-07	0.201762	0.101762	0.006	0.031746032	9.04858E-09
180	3.19E-06	6.35E-07	0.203286	0.109286	0.012	0.063492063	8.7519E-09
240	4.25E-06	8.46E-07	0.201952	0.111952	0.016	0.084656085	8.55412E-09
300	5.31E-06	1.06E-06	0.199333	0.115333	0.022	0.116402116	8.25744E-09
600	1.06E-05	2.12E-06	0.185238	0.132238	0.053	0.28042328	6.72462E-09
1200	2.12E-05	4.23E-06	0.169	0.16	0.097	0.513227513	4.54901E-09
1800	3.19E-05	6.35E-06	0.155524	0.179524	0.13	0.687830688	2.9173E-09
2400	4.25E-05	8.46E-06	0.147	0.191	0.15	0.793650794	1.92838E-09
3000	5.31E-05	1.06E-05	0.140667	0.200667	0.166	0.878306878	1.13725E-09
3600	6.37E-05	1.27E-05	0.135952	0.205952	0.176	0.931216931	6.42795E-10
5400	9.56E-05	1.90E-05	0.129333	0.210333	0.187	0.989417989	9.88915E-11
7200	1.27E-04	2.54E-05	0.128714	0.211714	0.189	1	0

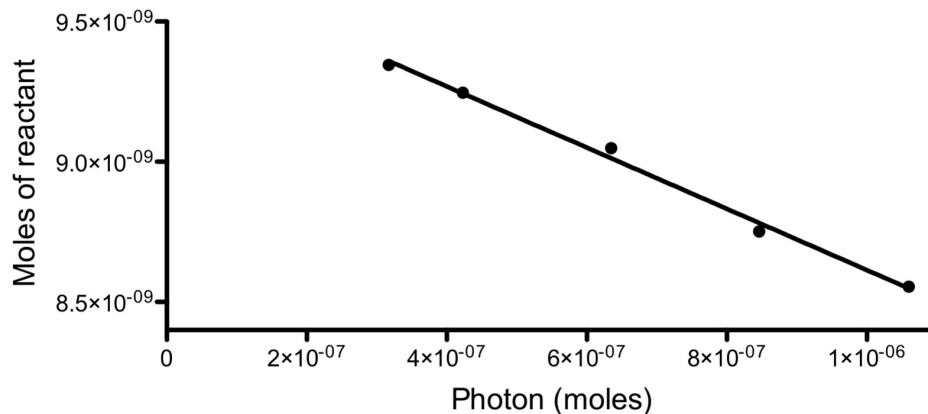


**Figure S25.** Linear regression for moles of reactant vs. moles of photons absorbed for Step 2 (complex **3**). Note that the photons used in Step 1 are not included in this photochemical reaction.

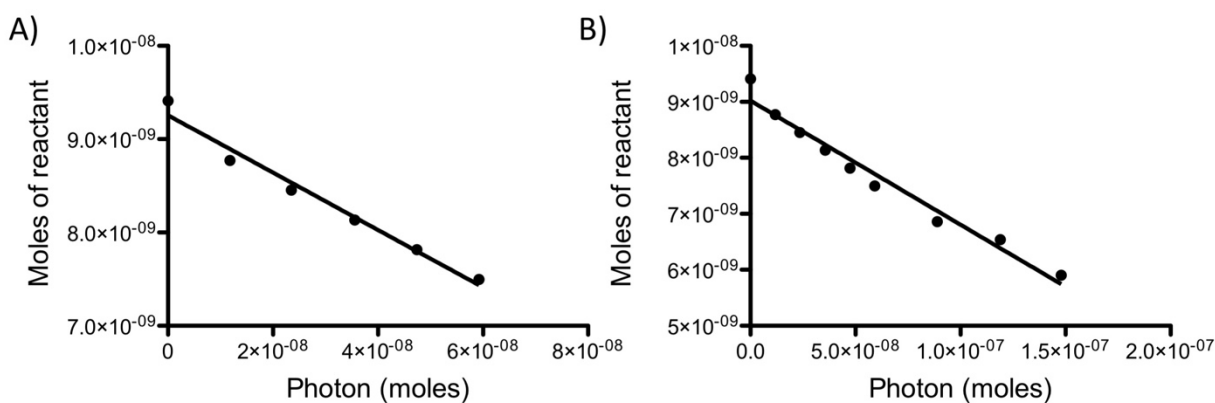


**Figure S26.** Comparison demonstrating the impact of including different numbers of time points on the determination of the quantum yield for compound **1**. A) The first 5 time points were used, giving  $\phi_{PS} = 0.031$ . B) The first 8 time points were used, giving  $\phi_{PS} = 0.022$ . The inclusion of additional data points in what appears to be the linear region can have a significant impact on the evaluation of the quantum yield.

The quantum yields for photosubstitution of complex **3** (Step 1 and 2) was also calculated based on HPLC.

Complex **3** (50  $\mu\text{M}$ ) was irradiated in 200  $\mu\text{L}$  aliquots under the same condition as for UV/Vis experiment, and 20  $\mu\text{L}$  were then injected for HPLC analysis. The initial *Area* (area under the curve in the chromatogram) corresponds the maximum moles of complex **3**. The decrease in the number of moles of complex **3** was calculated based on the decrease of the *Area* over time using the equation:

$$mol(t) = Area(t) * mol(init) / Area(init)$$

Were,  $mol(t)$  is moles of complex **3** at certain time point ( $t$ ),  $Area(t)$  is the  $Area$  at the same time ( $t$ ),  $mol(init)$  is the initial moles of compound **3** injected, and  $Area(init)$  is the initial  $Area$  for complex **3** before irradiation.

Finally, the moles of complex **3** irradiated in the 96-well plate were multiplied by 10 (volume irradiated is 200  $\mu$ L, volume injected is 20  $\mu$ L).

Considering that the absorption of the photoproduct  $[Ru(bpy)_2(pym)(H_2O)]^{2+}$  at 280 nm (the HPLC detection wavelength) could be different from the absorption of  $[Ru(bpy)_2(pym)_2]^{2+}$ , the correlation between  $Area$  and moles for photoproduct has been calculated as follows:

$$mol(product) = mol(5 s) - mol(init)$$

Were  $mol(product)$  is moles of product at time point 5 s,  $mol(5 s)$  is moles of complex **3** after 5 s irradiation, and  $mol(init)$  is the initial moles of compound **3** before irradiation. The moles of photoproduct at the following time points have been calculated by the same equation as for complex **3**.

**Table S12.** Parameters used in determining the quantum yield of **3** by HPLC.

Time	Photons absorbed	$[\text{Ru}(\text{bpy})_2(\text{pym})_2]^{2+}$			$[\text{Ru}(\text{bpy})_2(\text{pym})(\text{H}_2\text{O})]^{2+}$		
		Area	Moles injected	Moles in well	Area	Moles injected	Moles in well
0	0.00E+00	915.8	0.000000001	0.000000001	0	0	0
5	2.51E-08	656.8	7.17187E-10	7.17187E-09	245.2	2.82813E-10	2.82813E-09
10	5.03E-08	466.1	5.08954E-10	5.08954E-09	452.3	5.21681E-10	5.21681E-09
20	1.01E-07	197.8	2.15986E-10	2.15986E-09	645	7.43941E-10	7.43941E-09
30	1.51E-07	89.4	9.76196E-11	9.76196E-10	714.1	8.2364E-10	8.2364E-09
45	2.26E-07	34	3.7126E-11	3.7126E-10	751.5	8.66778E-10	8.66778E-09
60	3.68E-07	0	0	0	746.1	8.60549E-10	8.60549E-09
120	7.35E-07				658.6	7.59627E-10	7.59627E-09
180	1.10E-06				589.2	6.79581E-10	6.79581E-09
300	1.84E-06				521	6.0092E-10	6.0092E-09
600	3.68E-06				303.2	3.4971E-10	3.4971E-09
900	5.52E-06				161.8	1.8662E-10	1.8662E-09
1200	7.35E-06				89.8	1.03575E-10	1.03575E-09
1800	1.10E-05				55	6.34368E-11	6.34368E-10

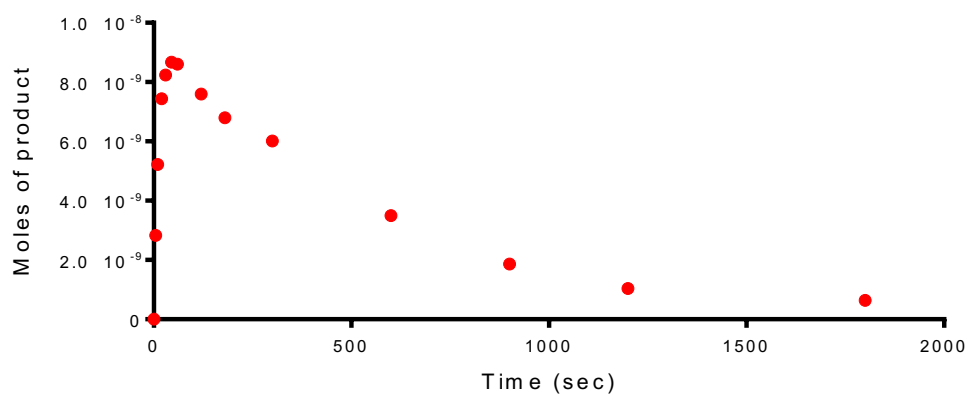


**Figure S27.** Moles of  $[\text{Ru}(\text{bpy})_2(\text{pym})(\text{H}_2\text{O})]^{2+}$  upon irradiation detected by HPLC.

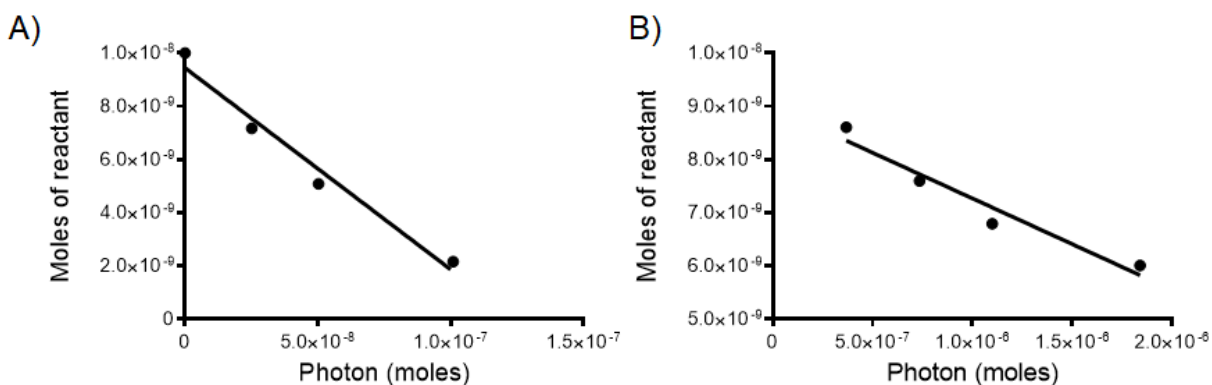


**Figure S28.** Linear regression for moles of reactant vs. moles of photons absorbed for complex **3** based on HPLC: A) Step 1, and B) Step 2.

**Table S13.** Photophysical parameters and quantum yields determined by different techniques.

Cmpd	$\lambda_{\max}$ abs (nm)		Half-life (min)		$\Phi_{PS}$ (using actinometer) <sup>a</sup>		$\Phi_{PS}$ (using power meter)	
	A	B	$t_{1/2}$ (1)	$t_{1/2}$ (2)	(1)	(2)	(1)	(2)
<b>1</b>	455	-	0.56	-	0.031	-	0.0175	-
<b>2</b>	420	450	0.17	47.88	0.11	0.0005	0.0617	0.00025
<b>3</b>	415	460	0.48	17.14	0.070 <b>0.059*</b>	0.0011 <b>0.0013*</b>	0.036 <b>0.032*</b>	0.00079 <b>0.00084*</b>
<b>4</b>	405	445	0.60	10.18	0.11	0.0033	0.059	0.00182
<b>5</b>					0.022	-	0.012	-
<b>6</b>					nd	nd	nd	nd
<b>7</b>					nd	nd	nd	nd
<b>8</b>			450		nd	-	nd	-
<b>9</b>			10.88		0.007	-	0.0036	-

<sup>a</sup> Value shown in manuscript.

## References

1. Howerton, B. S.; Heidary, D. K.; Glazer, E. C., *J. Am. Chem. Soc.* **2012**, *134* (20), 8324-7.
2. Wachter, E.; Zamora, A.; Heidary, D. K.; Ruiz, J.; Glazer, E. C., *Chem. Commun.* **2016**, *52* (66), 10121-4.
3. APEX2, Programs for data collection and data reduction. Bruker-Nonius: Madison WI. USA, 2012.
4. Krause, L., Herbst-Irmer, R., Sheldrick, G.M., Stalke, D., *J. Appl. Cryst.* **2015**, *48*, 3-10.
5. Parkin, S., Moezzi, B., Hope, H., *J. Appl. Cryst.* **1995**, *28*, 53-56.
6. Sheldrick, G. M., *Acta Cryst* **2015**, *A71*, 3-8.
7. Sheldrick, G. M., *Acta Cryst* **2015**, *C71*, 3-8.
8. Spek, A. L., *Acta Cryst* **2009**, *D65*, 148-155.
9. Parkin, S., *Acta Cryst* **2000**, *A56*, 157-162.
10. Kohler, L.; Nease, L.; Vo, P.; Garofolo, J.; Heidary, D. K.; Thummel, R. P.; Glazer, E. C., *Inorg. Chem.* **2017**, *56* (20), 12214-12223.
11. Hitchcock, P. B.; Seddon, K. R.; Turp, J. E.; Yousif, Y. Z.; Zora, J. A.; Constable, E. C.; Wernberg, O., *J. Chem. Soc., Dalton Trans.* **1988**, (7), 1837-1842.
12. Oktavia, B.; Lim, L. W.; Takeuchi, T., *Anal. Sci.* **2008**, *24* (11), 1487-92.
13. Hatchard, C. G.; Parker, C. A., *Proceedings of the Royal Society of London. Series A. Mathematical and Physical Sciences* **1956**, *235* (1203), 518-536.
14. Marcolongo, J. P.; Schmidt, J.; Levin, N.; Slep, L. D., *PCCP* **2017**, *19* (32), 21373-21381.
15. Pinnick, D. V.; Durham, B., *Inorg. Chem.* **1984**, *23* (10), 1440-1445.
16. Liu, Y.; Turner, D. B.; Singh, T. N.; Angeles-Boza, A. M.; Chouai, A.; Dunbar, K. R.; Turro, C., *J. Am. Chem. Soc.* **2009**, *131* (1), 26-+.
17. Chan, H.; Ghrayche, J. B.; Wei, J.; Renfrew, A. K., *Eur. J. Inorg. Chem.* **2017**, *2017* (12), 1679-1686.
18. Bahreman, A.; Cuello-Garibo, J. A.; Bonnet, S., *Dalton Trans* **2014**, *43* (11), 4494-505.
19. Smith, N. A.; Zhang, P.; Greenough, S. E.; Horbury, M. D.; Clarkson, G. J.; McFeely, D.; Habtemariam, A.; Salassa, L.; Stavros, V. G.; Dowson, C. G.; Sadler, P. J., *Chem Sci* **2017**, *8* (1), 395-404.